Title: Heat transfer in plagioclase feldspars
Authors: Joy M. Branlund and Anne M. Hofmeister

Abstract
Laser Flash Analyses (LFA) of oriented sections of five natural plagioclase crystals provide thermal diffusivity (*D*) as function of temperature (to ~1300-1500 K) and composition (An_{5-65}). Plagioclase has low thermal diffusivity; over much of the solid solution room temperature *D* is 0.979 to 0.751 mm^2/s along **c**, 0.919 to 0.767 mm^2/s along **b**, and 0.632 to 0.868 mm^2/s perpendicular to **b** and **c**. The directionally averaged *D* is 30-45% lower than *D* of Amelia albite. Thermal conductivities calculated using measured *D* values are almost the same for all samples of An>18, being about 1.5 - 1.9 $Wm^{-1}K^{-1}$ and changing little with temperature. Increasing Al-Si disorder causes *D* to decrease with increased An content, although sample structure causes more ordered samples to have higher *D* than more disordered samples. Inflections in *D*(*T*) are connected with structural changes with *T*. Disordering with increased temperature or change to a $C\bar{1}$ structural component lowers *D*. Structure dictates whether *D* along the **b** axis is greater or less than that along **c**, possibly because ordering in An-like domains increases *D* along **c** relative to **b**. Likewise, disorder during heating decreases *D* in albite along **c** but has little impact on *D* in the other directions. The anharmonic lattice effects that dictate both thermal expansivity and *D* are swamped by effects of disorder; the latter plays a major role in heat transport in plagioclase. Our measurements indicate that plagioclase is more insulating than other major igneous rock-forming minerals. Thermal diffusivity of major rock-forming minerals appear to depend on numbers of IR modes, a finding that suggests heat transfer is better described using electromagnetic waves traversing the solid than by a phonon scattering model.

Introduction

Solving many geologic problems requires understanding the thermal nature of Earth's crust and mantle, and thus knowledge of relevant mineral heat transfer properties (thermal conductivity (*k*) and thermal diffusivity (*D*)). Therefore, we have been building a database of mineral thermal diffusivities measured with Laser Flash Analysis (LFA). To date, several glass and mineral systems have been probed, including quartz, perovskite, olivine, clinopyroxene, orthopyroxene, garnet and spinel (Branlund and Hofmeister 2007; Hofmeister 2010; Pertermann and Hofmeister 2006, 2008; Hofmeister 2011, 2006, 2007). Data on low albite and low sanidine have been published (Pertermann et al. 2008; Hofmeister et al. 2009), but more-calcic plagioclase data are lacking. Given that feldspar is the most common rock-forming mineral, and plagioclase is prevalent in intermediate and mafic igneous rocks, it is especially important to characterize heat transfer in plagioclase.

Plagioclase minerals are structurally complex (Figure 1). At high temperature, a true solid solution exists between the sodic and calcic end members of the plagioclase series, albite ($NaAlSi_3O_8$) and anorthite ($CaAl_2Si_2O_8$). Low albite is ordered such that Al always resides on the T_1O site, forming a $C\bar{1}$ structure. With increased temperature, Al can diffuse to other sites and albite disorders, forming high albite (still $C\bar{1}$). At a higher temperature, the framework shears leading to a partially ordered monoclinic structure (*C2*/*m* space group) (Parsons 2010). In pure anorthite, each Al is surrounded by four Si and vice versa; the alternating layers of Si and Al tetrahedra double the length of the **c**-axis in the crystallographic unit cell (McConnell 2008); Like low albite, anorthite exhibits long-range order. Unlike albite, anorthite remains perfectly ordered (with the $I\bar{1}$ structure) until melting. At low temperature (below about 500 K), The anorthite lattice distorts around Ca atoms, creating a $P\bar{1}$ structure. Charge imbalances caused by

Na-Ca substitution in anorthite-albite are counteracted by Al-Si exchange. Atomic ordering becomes complicated because Al-O-Al bonds are energetically expensive; intermediate plagioclase therefore consist of planar subdomains with slightly different structures, and these antiphase domains combine to form incommensurate superstructures. The two main intermediate structures are the more Ab-rich e_2 and the more An-rich e_1 plagioclase, so named because of *e* reflections that appear in single-crystal x-ray photographs. McConnell (2008) proposed that e_2 plagioclase contains alternating domains of albite-like ($C\bar{1}$) and an anorthite-like ($I\bar{1}$) structures, whereas the e_1 phase contains alternating incommensurate layers of ordered and partially ordered $I\bar{1}$ structures. The widths of the domains are on the order of 20-50 nm, and orientations vary with An-content and temperature (e.g., Carpenter 1991; Grove 1977). At low temperatures, miscibility gaps exist in the solid solution, and intergrowths of the different structures form, creating peristerite ($C\bar{1}$ and e_2), Bøgglid (e_1 + e_2) and Hüttenlocher (e_1 + $I\bar{1}$) intergrowths (Figure 1). It is likely that the entire solid solution, with the exception of the two end members, is immiscible at temperatures (<~400 K) (Parsons 2010).

Because atomic diffusion is very sluggish in plagioclase, many samples retain a metastable structure (either $C\bar{1}$, $I\bar{1}$, e_1 or e_2) upon cooling. Only very slowly cooled plutonic samples and metamorphic samples will possess the intergrowths, whereas volcanic plagioclase are more disordered with structures that may reflect high temperature solid solution. Plagioclase therefore does not simply fall into a “high” versus “low” category, but exhibits a wide range of order-disorder reflecting varied cooling histories.

In this study, we measure thermal diffusivity of natural plagioclase with compositions ranging from An_5 to An_{65} at different temperatures, thus quantifying heat transfer for several different plagioclase chemistries and structures.

Methods

Samples

Low albite from Amelia County, Virginia, was previously studied along with Ab and An glasses (Hofmeister et al. 2009; note, the low albite was mistakenly called high albite in that paper). To this we add data from seven natural plagioclase samples with higher An contents, five of which were analyzed to high temperature (Table 1).

An anorthite mat was fabricated by cooling a synthetic $CaAl_2Si_2O_8$ glass (see Hofmeister et al. 2009). The resulting sample is fine grained and polycrystalline, probably containing some glass.

Each crystal was cut along three orthogonal directions. Two sections were cut parallel to (001) and (010). A third section cut perpendicular to these two faces is designated "⊥" because plagioclase is triclinic; the perpendicular face is not (100). Values presented for (001) therefore quantify heat flow along **c** while (010) quantifies heat flow along **b**. Although **a** is almost perpendicular to **b**, it is oblique to **c** (angles range from 115.5°-116.3°), thus the perpendicular orientation does not quantify heat flow along **a**.

Sections were ground into discs about 1 cm in diameter and less than 1 mm thick. The top and bottom of each disc were polished to be parallel. Optical microscopy was used to identify any inclusions and twinning. Before analyzing *D*, samples were sputter coated with platinum and then spray coated with graphite. The graphite coating maximizes energy absorption, and ensures that absorbed energy is spread across the surface. The platinum coating helps reduce the amount of direct (or ballistic) radiation through these transparent samples.

Chips from each sample were analyzed using wavelength-dispersive analysis (WDS) on

the JXA-8100 electron microprobe at Washington University in St. Louis to quantify major element chemistry. Accelerating voltage was 15 kV, beam current was nominally 25 nA, beam diameter was 1 μm, and counting times were near 30 s. Various oxide standards were used for calibration. Measurements of three points were averaged to give the chemical formulas of plagioclase samples (Table 1).

Measurement of thermal diffusivity

Thermal diffusivity was measured with the Netzsch LFA427, a laser-flash apparatus. The instrument heats the sample's base briefly with a laser pulse, and records changes in emissions from the top of the sample using a remote IR detector. Basically, *D* is calculated using the time taken for the heat from the pulse to travel through a sample of given thickness. This technique is preferred because no contacts exist between thermocouples and the sample; such contacts limit measurements to ~1200 K and provide an additional thermal resistance that artificially lowers measured *D* values. LFA accounts for the shape of the laser pulse and removes unwanted ballistic radiative transfer using the mathematical model of Mehling et al. (1998). For details, see Pertermann and Hofmeister (2006).

Thermal diffusivities of plagioclase samples were measured at 100 K increments from room temperature up to between 1150-1550 K. At each temperature step, at least three measurements were collected and averaged. Measurements with poor fits between the model and signal were not included in the average. Graphs presented herein show the average of successful measurements. Due to its small size, *D* of sample FSU⊥ could only be measured at room temperature. Samples FLT and FLC were also measured only at room temperature.

Results

Plagioclase *D* generally decreases with temperature (Figure 2) and can be fit with a third-order polynomial, namely:

$$D = \frac{1}{A + BT + CT^2 + ET^3} \quad (1)$$

Coefficients for the different samples are given in Table 2.

Thermal diffusivity decreases with increased An content (Figure 3). For intermediate values of An, the *D* values are very similar; from An_{19} and An_{65}, room temperature *D* decreases from 0.979 to 0.751 mm^2/s along **c** and 0.919 to 0.767 mm^2/s along **b**. For comparison, *D* along **b** in pure albite is 1.689 mm^2/s (Hofmeister et al. 2009). Albite's measured value of *D* along **c** of 1.354 mm^2/s is likely too low, because that section was cut too thick, and therefore lost heat through the sample edges. Fracturing along cleavages prohibited preparation of a thinner sample. Thermal diffusivity of the anorthite mat is lower than the true anorthite value due to glass present in the polycrystalline sample. Because the anorthite primitive unit cell contains the same number of formula units as albite, *D* should be continuous across the series. Extrapolation of plagioclase data to higher An gives a *D* value (averaged over the three directions) for pure anorthite of 0.741 mm^2/s at room temperature and about 0.574 at high temperature (about 1100 K).

For albite, even considering possible errors due to sample thickness, *D* along **b** (measured using (010) sample) is higher than along **c** for all temperatures measured (Figure 2a; Hofmeister et al. 2009). This is not the case for all other plagioclase samples studied. Like albite, *D* in sample FSU is significantly higher along **b** than **c** (Figure 2b). Although samples FLL and FBM also have greater *D* along **b** than **c**, *D* values are difficult to distinguish given experimental uncertainty, at least within certain temperature ranges. For sample FBM, D_{010} and D_{001} are

similar from room temperature up to 768 K, such that *D* values diverge as temperature increases (Figure 2a). Samples FON and FLN both had $D_{001}>D_{010}$ at lower temperatures, although the *D* values crossed over, so that $D_{010}>D_{001}$ at higher temperatures.

Except for FON and FLN, samples did not change appearance when compared before and after heating in the LFA. During LFA analysis, sample FON was heated above its melting temperature. At about 1580 K, large peaks of direct radiation were detected in FON001 and FON⊥, suggesting that these samples cracked, probably during the growth of lower density melt pockets. Although intact, both samples were netted with two sets of microscopic fractures that formed at angles between 40° to 60° from the **a-c** plane. FON001 had a higher density of cracks, as well as two larger cracks, one ending in a conchoidal fracture, near the sample's edge. There was no evidence wholesale flow (no change in sample shape, for example). However, inclusions visible in this sample pre-heating were not visible after LFA runs, and chains of dark, small dots (glass) appeared mostly along (001) cleavages in FON⊥ and along fractures in FON001.

Thermal diffusivity decreases or is constant with temperature at all temperatures measured with three exceptions. Thermal diffusivity increases significantly above 1300 K in FLN001 and FLN010 (*D* increases 7-11% from 1320 to 1420 K) (Figures 2b and 4). Furthermore, additional measurements made on cooling show that in both FLN001 and FLN010, *D* remained higher upon cooling, at least until a temperature of ~800 K. Sample FLN⊥ was not analyzed to as high a temperature as the other two orientations; it might very likely show a similar increase in *D* if analyzed at higher temperatures. The recovered sample contains two sets of fractures, one which lines up with ilmenite inclusions. FLN⊥ also cracked during analysis. The samples likely cracked on cooling, explaining the lower *D* measured during cooling below

~800 K. The cracks also lead to lower room temperature *D* measured at a later date (diamond and plus sign in Figure 4).

Sample FON001 has a 5% increase in *D* from 1260 to 1460 K (filled gray circles in Figure 2a). That D_{001} increases following premelting from 1260 to 1460 K may result from dehydration.

Thermal diffusivity and plagioclase structure

Thermal diffusivity measurements may provide additional insights on plagioclase structure, the complexity of which is compounded by the sluggish kinetics (several samples retain their high temperature structures) and possible effects of variable amounts of K subsituting for Na, or for Fe in either cation site, as well as small amounts of water or hydroxyl.

Thermal diffusivity of albite is much higher than *D* of other members of the plagioclase series. Likewise, albite is the only sample analyzed that should be well ordered at room temperature. The addition of Al reduces order, and hence reduces *D*. Likewise, in intermediate plagioclase, more ordered samples (FON, FLN, FLC) have higher room temperature *D* than the more disordered samples (FLL and FBM) (Figure 3).

The direction of maximum *D* seems to depend on plagioclase structure (Figure 1b). For samples with $C\bar{1}$ symmetry, $D_{010}>D_{001}$. For all other structures, $D_{001}>D_{010}$. In phases with a $C\bar{1}+e_2$, the direction of maximum *D* depends on the relative amounts of the two phases, which depends on An content. Samples with low An content such as FSU (An_5) will have $D_{010}>D_{001}$, whereas samples with higher An content such as FON (An_{19}) will have $D_{001}>D_{010}$. The division between these high and low An contents corresponds to the position of the $C\bar{1} \leftrightarrow e_2$ boundary extrapolated to lower temperatures. The switch in orientation of maximum *D* may suggest that

ordering associated with development of the anorthite-like component of the superstructure increases *D* preferentially along **c**. This would occur if antiphase domains orient such that **c** resides almost entirely in the more-ordered domain.

Several of the inflections and crossovers in the $D^{-1}(T)$ plots correspond to changes in the plagioclase structure. Albite $D^{-1}(T)$ can be fit linearly, as long as the lines break at about 625 K, a temperature that may mark the high-low albite boundary as the sample disorders upon heating (Figure 5a). The transition seen in LFA is lower than the equilibrium transition in Figure 1. Of the transitions in the phase diagram, only the low to high $C\bar{1}$ transition does not involve a symmetry change. Similar to the way that LFA "sees" melting at different temperatures than do other techniques, such as viscosimetry (Hofmeister et al. 2009), LFA "sees" the low to high $C\bar{1}$ transition at a lower temperature than other techniques. The variation on *T* at which transitions are detected result from relaxation timescales differing among experimental techniques. In (010), a second inflection occurs at about 1300 K which could mark the transition from $C\bar{1}$ to *C2/m*. Given that this transition is accompanied by a symmetry change, the LFA inflection and equilibrium transition temperature are similar.

In FSU, small inflections at ~850 K in both orientations are close to the transition from low $C\bar{1}+e_2$ to $C\bar{1}$ (Figure 5b). The inflection at ~1250 K in $D^{-1}{}_{010}(T)$ occurs where expected for the $C\bar{1}\leftrightarrow C2/m$ transition (1290 K; McConnell 2008). Inflections at about 1050 K in the $D^{-1}(T)$ plots for both (010) and (001) may reflect that the phase transition is gradual, the sample becoming more like *C2/m* with heating as proposed by Prewitt et al. (1976).

The peristerite intergrowths in FON will not diffuse during the brief heating times of the LFA. However, the two components may disorder. If the more Ab-rich component (with a low $C\bar{1}$ structure) disorders at a different temperature that the intermediate e_2 structure, multiple

inflections could exist in the data. An inflection in all orientations at ~800 K corresponds to the expected change from $e_2 \leftrightarrow C\bar{1}$ (Figure 5c). There is also an inflection in the plot for $D_{\perp}$ at ~600 K, which may represent the disordering of the $C\bar{1}$ component.

The crossover of D_{010} and D_{001} also results from the change in structure to $C\bar{1}$ symmetry, even though the crossover temperature for sample FON is hard to pinpoint. The measured *D* values for FON001 are slightly larger to 868 K, and by 976 K diffusivity is larger along (010) than along (001), but error bars for *D* along the two orientations overlap between 378 and 996 K.

Thermal diffusivity of FON001 and FON⊥ drop drastically between 1200 and 1300 K., while D_{010} decreases slightly at the same temperature. The melting temperature for this composition is about 1400 K (McConnell 2008). Although the presence of OH and K will lower the solidus (Johannes et al. 1994; Parsons 2010), the decrease in *D* is consistent with the glass transition as seen by the LFA occurring at temperatures about 100 K lower than the melting temperature (Hofmeister et al. 2009). Because the melting temperature of plagioclase increases with An-content (Figure 1), the more Ab-rich component of the peristerite intergrowth will melt first. Because peristerite intergrowths parallel ~(010), melt will form in the **a-c** plane, and therefore affect $D_{\perp}$ and D_{001} more than D_{010}. As further evidence for differential melting of peristerite, melt (as beads of glass seen in recovered samples) aligns with the (001) cleavage in FON⊥. Beads of glass do not align with (100) in FON001, but follow fractures. This might be expected if melt formed along **a** but then accumulated in fractures. At 1460 K, enough melt exists to crack the sample, allowing direct radiation through the sample that aborted the run.

The crossover temperature of FLN is about 850 K, which matches the predicted transition from the Bøgglid intergrowth (e_1+e_2) to a high $C\bar{1}$ structure (about 886 K) (Figure 5d). The e_1 portion of the structure should alter to $C\bar{1}$ at a lower temperature than the e_2 phase, which

explains the width of the transition in temperature space. Above this temperature (in the $C\bar{1}$ stability field), *D* of FLN is considerably lower than for other samples (Figure 2b), until about ~1400 K, where *D* of both orientations increase to values similar to the other plagioclase samples of about 0.6 mm^2/s. Some aspect of FLN's structure, perhaps the Bøgglid intergrowths, restricts *D*. As temperature increases, the structure flexes, returning to that expected for $C\bar{1}$ plagioclase with intermediate An values by 1600 K. The thermal history of the sample might also be responsible for the reset of *D* at high temperature. Although originally plutonic, the slowly-cooled anorthosite intrusions were later metamorphosed. Strain imparted during metamorphism might have overprint the lattice in a manner that affects *D*.

There are no clear inflections in the $D^{-1}(T)$ plots for sample FBM (Figure 5e). D_{010} is greater than D_{001} at all temperatures, implying that this sample has a $C\bar{1}$ structure, and cooled quickly enough to preserve that $C\bar{1}$ structure.

In sample FLL, D_{010} appears to exceed D_{001} at room temperature and above 1400 K (Figure 5f). However, the error bars for D_{001} and D_{010} in sample FLL overlap at room temperature and again at temperatures greater than 1100 K. Unlike the other samples, $D_{\perp}$ is similar to the other orientations, being in between D_{001} and D_{010} at temperatures below 1000 and above 1400 K, but lower than D_{001} and D_{010} between those temperatures. The temperatures of the 1400 K crossover corresponds to the transition between the $I\bar{1}$ and $C\bar{1}$ structures, and the crossover is due mainly to a decrease in D_{001}. In addition to the inflection at 1400 K in $D^{-1}(T)_{001}$ and $D^{-1}(T)_{\perp}$, possible inflections exist at ~1160 K in $D^{-1}(T)_{010}$, and at ~1250 K in $D^{-1}(T)_{001}$. Despite the fact that FLL is a volcanic sample, the inflections at ~1200 K correspond to the expected transition to an e_1 structure, and suggest that when the crystal formed, cooling was slow enough for this sample to weakly order. The Lake County Labradorite cooled within a thick

basaltic lava flow, which also explains the weak *e* reflections in the single-crystal x-ray photographs (Wenk 1980). Possible inflections at 600 K in $D^{-1}(T)_{010}$ and 800 K in $D^{-1}(T)_{\perp}$ and $D^{-1}(T)_{001}$ are unexplained, but could reflect a disordering of one of the antiphase domains in the e_1 structure. A further decrease of D_{001} as temperatures approach 1600 K result from premelting effects.

Thermal diffusivity and thermal expansivity

The volume coefficient of thermal expansion (α_V) was calculated for different members of the plagioclase series from measured volumes from Hovis et al. (2010) and Tribaudino et al. (2010), using:

$$\alpha_v = \frac{1}{V_0}\frac{\partial V}{\partial T} \qquad (2)$$

where V_0 is the volume at room temperature. Linear fits to $V(T)$ were appropriate and used to compute α_V. To determine dependence of α_V on An content, the two variables were plotted and linearly fit, using different fits for An<40 and An>40 (not shown).

Values of room temperature D^{-1} are compared with α_V in Figure 6. As seen by the disagreements of values calculated from different volume data, large uncertainty exists in α_V (Figure 6). Nonetheless, a clear trend shows that samples with lower thermal expansion coefficients have higher D^{-1} (lower D) values. This is opposite of what was seen in halides (Yu and Hofmeister 2011) and endmember perovskites (Hofmeister 2010), where α_V and D^{-1} are positively correlated. In those minerals, higher α means the lattice is more responsive to temperature, hence causing more phonon scattering and higher D^{-1}. In plagioclase, disorder has

reversed the trend. Samples with An>40 plot along different trends than do more sodic samples. Although offset, the trends do have similar slopes. The different trends reflect the different structures for minerals with these An contents; this break is generally the boundary between $C\bar{1}$ and $I\bar{1}$. Although lattices of more An-rich samples should be less responsive to *T*, effects of higher amounts of Al-Si disorder swamp the lattice impact on *D*.

Directional $D^{-1}(T)$ should go as $\alpha_L T$, reflecting the fact that both are governed by anharmonic effects. Because thermal changes in length are small, α_L is most accurate in the middle of the temperature range. Therefore, lengths of **a**, **b** and **c** for albite (Tribaudino et. al 2010) were plotted at temperatures >500 K and linearly fit.

For the (010) and ⊥ samples, $\alpha_L T$ and $D^{-1}(T)$ increase similarly with temperature, as expected (Figure 7). This behavior was similarly seen in perovskites and halides (Hofmeister 2010; Yu and Hofmeister 2011). The slope of $\alpha_L T$ for the **c** orientation is much less than that for $D^{-1}(T)$, which causes $\alpha_L T$ along **a**>**b**>**c**, but D^{-1} along **a**>**c**>**b**. The mismatch in slopes for the (001) sample indicates that additional phonon scattering, probably due to disorder upon heating and not the expected lattice effect, enhances D^{-1} along this orientation. That disordering decreases *D* in albite mimics the fact that ordering (due to formation An-like domains, for example) increases *D* preferentially along **c**.

Thermal conductivity

Bulk thermal diffusivities of samples were calculated using:

$$D = \left[\frac{1}{3} \left(\frac{1}{D_x} + \frac{1}{D_y} + \frac{1}{D_z} \right) \right]^{-1} \qquad (5)$$

where D_x, D_y and D_z are diffusivities along three orthogonal directions.

Thermal conductivity (k) is then calculated as:

$$k = D\frac{c_p}{\rho} \quad (6)$$

Heat capacities vary only slightly for different members of the plagioclase solid solution (Figure 8). Nonetheless, thermal conductivities were calculated using An-specific heat capacity values from Benisek et al. (2009). Densities were calculated using temperature-dependent molecular volumes, which were assumed to vary linearly with An content, using albite and anorthite values from Holland and Powell (1998). Thermal conductivities are not very sensitive to the choice of density. Measured volumes from Tribaudino et al. (2010) give very similar k values. The resulting thermal conductivity values change little with temperature for all but the most albite-rich plagioclase (Figure 8).

Comparison with previous measurements of plagioclase and other major rock-forming minerals

Although albite and potassium feldspar minerals have been previously analyzed, measurements of plagioclase heat transfer properties are rare in the literature. An exception is a study by Magnitskiy (1971) of a labradorite (density of 2.67 g/cm^3) and an oligoclase (density of 2.63 g/cm^3). Specific An contents were not reported. Thermal diffusivities were measured to 1200 K with plane-periodic wave method, which involves one thermocouple attached to the sample; the samples were not oriented crystals. Their data is in decent agreement with our measurements; the oligoclase values are slightly higher than ours to 800 K, and their labradorite

values are on the low end of our labradorite measurements at temperatures up to 1000 K (Figure 9).

Linvill (1987) measured thermal diffusivity of Madagascar albite ($Ab_{99}An_1$, ρ=2.622), Nain labradorite ($Ab_{48.7}An_{48}Or_{3.3}$, ρ=2.695), Lake St. John labradorite ($Ab_{33}An_{65.5}Or_2$), and Lake County labradorite ($Ab_{31}An_{68}Or_1$, ρ=2.71) at low temperatures using a divided bar technique and to about 500 K using the modified Ångstrom method. The long axes of the samples were 010 in albite, $11\bar{2}$ in the Nain sample, and $20\bar{3}$ in the Lake County sample. Orientations for the Lake St. John sample were not given. Data from attained with the modified Ångstrom method are shown in Figure 9. Lake County and Lake St. John data are slightly lower than ours, and data from the Nain labradorite are higher than ours, due to various amounts of radiative gains and contact losses.

When compared with other common rock-forming minerals, plagioclase has one of the lowest thermal diffusivities, both at room temperature and higher temperatures (Figure 10). Of the major families of rock-forming minerals, quartz and olivine have the highest thermal diffusivities. In general, thermal diffusivity is linked to the number of active infrared (IR) modes in a mineral along the direction probed, which is determined by number of atoms and structure in a given unit cell. Quartz and olivine have few modes compared to orthopyroxene and garnets, and thus plot higher in Figure 10. Interestingly, the correlation is not with the number of optic modes, but only with IR modes, and the degeneracy of the IR modes is not relevant (e. g., garnet has 237 optic modes, considering degeneracies). It is the individual peaks that have an effect. Infrared modes involve a change in dipole moment, unlike Raman or inactive modes. Our finding suggests that heat propogation can be described as an electromagnetic wave traversing the sample. That is, the behavior is similar to “light” or optics experiments. Phonon scattering

has been the standard model to explain heat transfer in solids since the time of Debye and Einstein, but this model does not explain the trend in Figure 10.

Conclusions

Laser-flash analysis of plagioclase feldspars reveals clues about the feldspar structure, as inflections in the *D(T)* curves occur at temperatures expected for phase transitions. Fast heating and cooling during LFA measurements do not allow for atomic diffusion, but nonetheless are tied to structural changes to the tetrahedral framework. In all minerals, *D* decreases upon heating as more phonons lead to increased phonon scattering. Plagioclase *D* is further affected by disordering upon heating. For example, *D* drops in all samples during the transition to $C\bar{1}$ symmetry.

Likewise, disorder accompanying Al/Si substitution causes *D* of plagioclase to decrease with increasing anorthite content. The decrease seems mostly continuous across the solid solution, regardless of the crystallization temperature and/or cooling history of the sample. This suggests that ordering/disordering dictated by structure at a given composition is minimal compared with ordering/disordering dictated by An contents.

Application of our results to geological problems is straightforward. First, thermal conductivity values for plagioclase can easily be approximated. When combined with heat capacity and density, *D* give similar room temperature thermal conductivity values (between about 1.5 and 1.9 $Wm^{-1}K^{-1}$) for all plagioclase samples containing some Ca. Also, thermal conductivity changes little with temperature. Secondly, that *D* is lower for plagioclase (at all temperatures) than for other major rock-forming minerals suggests that plagioclase will dictate lower bounds of *D* and *k* in plagioclase-bearing rocks, especially mafic rocks in Earth's crust.

Acknowledgements

We wish to thank Paul Carpenter at Washington University in St. Louis for performing microprobe analyses of our samples and Cathleen Brown, Museum Specialist at the Smithsonian for providing some samples. Thanks also to the National Science Foundation, whose grants #0711020 and #091142 funded this research.

References

Angel, R. J., Carpenter, M. A. and Finger, L. W. (1990) Structural variation associated with compositional variation and order-disorder behavior in anorthite-rich feldspars. American Mineralogist, 75, 150-162.

Benisek, A., Dachs, E. and Kroll, H. (2009) Excess heat capacity and entropy of mixing in high structural state plagioclase. American Mineralogist, 94, 1153-1161.

Branlund, J. M. and Hofmeister, A. M. (2007) Thermal diffusivity of quartz to 1000 °C: Effect of impurities and the α-β phase transition. Physics and Chemistry of Minerals, 34, 581-595.

Carpenter, M. A. (1994) Subsolidus phase relations of the plagioclase feldspar solid solution. In I. Parsons, Ed. Feldspars and their reactions. p. 221-270. NATO ASI Series C Vol. 421, Edinburgh.

Carpenter, M. A. (1991) Mechanisms and kinetics of Al-Si ordering in anorthite: I. Incommensurate structure and domain coarsening. American Mineralogist, 76, 1110-1119.

Carpenter, M. A. and McConnell, J. D. C. (1984) Experimental delineation of the $I\bar{1} \leftrightarrow C\bar{1}$ transformation in intermediate plagioclase feldspars. American Mineralogist, 69, 112-121.

Grove, T. L. (1977) A periodic antiphase structure model for the intermediate plagioclases (An_{33} to An_{75}). American Mineralogist, 62, 932-941.

Hofmeister, A. M. (2011) Thermal diffusivity of spectroscopically characterized orthopyroxenes as a function of temperature and chemical composition. Submitted to European Journal of Mineralogy.

Hofmeister, A. M. (2010) Thermal diffusivity of oxide perovskite compounds at elevated temperature. Journal of Applied Physics, 107, 103532 (20 pgs).

Hofmeister, A. M. (2007) Thermal diffusivity of aluminous spinels and magnetite at elevated temperature with implications for heat transport in Earth's transition zone. American Mineralogist, 92, 1899-1911.

Hofmeister, A. M. (2006) Thermal diffusivity of garnets at high temperature. Physics and Chemistry of Minerals, 33, 45-62.

Hofmeister, A. M., Whittington, A. G. and Pertermann, M. (2009) Transport properties of high albite crystals, near-endmember feldspar and pyroxene glasses, and their melts to high temperature. Contributions to Mineralogy and Petrology, 158, 381-400.

Holland, T. J. and Powell, R. (1998) An internally consistent thermodynamic data set for phases of petrologic interest. Journal of Metamorphic Petrology, 16, 309-343.

Hovis, G. L., Medford, A., Conlon, M., Tether, A. and Romanoski, A. (2010) Principles of thermal expansion in the feldspar system. American Mineralogist, 95, 1060-1068.

Johannes, W., Koepke, J. and Behrens, H. (1994) Partial melting reactions of plagioclases and plagioclase-bearing systems. In I. Parsons, Ed. Feldspars and their reactions. p. 161-194. NATO ASI Series C Vol. 421, Edinburgh.

Linvill, M. (1987) Glass-like thermal conductivity behavior in feldspars. PhD thesis, Cornell University, Ithaca, NY.

Magnitskiy, V. A., Petrunin, G. I. and Yurchak, R. P. (1971) Thermal diffusivity of selected microclines and plagioclases between 300 and 1200 degrees K. Dolkady: Earth Science Sections, 199, 25-27.

McConnell (2008) The origin and characteristics of the incommensurate structures in the plagioclase feldspars. The Canadian Mineralogist, 46, 1389-1400.

Mehling, H., Hautzinger, G. and Nilsson, O. and Fricke, J. and Hofmann, R. and Hahn, O. (1998) Thermal diffusivity of semitransparent materials determined by the laser-flash method: applying a new analytical model. International Journal of Thermophysics, 19, 941-949.

Parsons, I. (2010) Feldspars defined and described: a pair of posters published by the Mineralogical Society. Sources and supporting information. Mineralogical Magazine, 74, 529-551.

Pertermann, M. and Hofmeister, A. M. (2006) Thermal diffusivity of olivine-group minerals at high temperature. American Mineralogist, 91, 1747-1761.

Pertermann, M. and Hofmeister, A. M. (2008) Thermal diffusivity of clinopyroxenes at elevated temperatures. European Journal of Mineralogy, 20, 537-549.

Pertermann, M., Whittington, A. G., Hofmeister, A. M., Spera, F. J. and Zayak, J. (2008) Transport properties of low-sanidine single-crystals, glasses and melts at high temperature. Contributions to Mineralogy and Petrology, 155, 689-702.

Prewitt, C. T., Sueno, S. and Papike, J. J. (1976) The crystal structure of high albite and monalbite at high temperatures. American Mineralogist, 61, 1213-1225.

Tribaudino, M., Angel, R. J., Cámara, F., Nestola, F., Pasqual, D. and Margiolaki, I. (2010) Thermal expansion of plagioclase feldspars. Contributions to Mineralogy and Petrology, 160, 899-908.

Wenk, H-R., Joswig, W., Tagai, T., Korekawa, M. and Smith, Bradley K. (1980) The average structure of An 62-66 labradorite. American Mineralogist, 65, 81-95.

Yu, X. and Hofmeister, A. M. (2011) Thermal diffusivity of alkali and silver halide crystals as a function of temperature. Journal of Applied Physics, 109, 033516-1.

Figure captions

Figure 1

Phase diagram for plagioclase showing (a) major structures (modified from Parsons (2010) and McConnell (2008), with the low to high $C\bar{1}$ transition from Carpenter (1994)) and (b) the direction of maximum *D* for the different structures using measurements from the present study. Location of the $C\bar{1}/I\bar{1}$ boundary (heavy black line) agrees with data from Carpenter et al. (1984). Pe, Bø, Hü are the peristerite, Bøgglid and Hüttenlocher intergrowths, respectively. More uncertainty exists in the low temperature portion of the diagram than in the upper due to sluggish kinetics. Locations of the upper phase boundaries are affected by Or contents. For example, adding K lowers *T* of the low to high $C\bar{1}$ transition as well as the solidus (Parsons 2010). The solidus decreases with increased P_{H2O} by up to 400 K (Johannes et al. 1994).

Figure 2

Thermal diffusivities versus temperature for (a) samples FON (filled gray), FBM (open black), and albite (filled black, from Hofmeister et al. (2009)), and (b) samples FLN (filled gray), FSU (filled black), FLL (open black) and anorthite mat (black diamonds). Measurements made on (010) are shown as squares, on (001) are shown as circles, and on perpendicular sections are shown as triangles. Error bars are included, but many are smaller than the symbol size. Larger error bars for albite (001) reflect uncertainty due to excessively large sample thickness.

Figure 3

Thermal diffusivity versus An content. Black symbols show values measured at room temperature, and gray symbols show values measured at about 1100 K. Measurements made on

(010), (001) and ⊥ are shown with squares, circles and triangles, respectively. The anorthite mat is polycrystalline (not oriented) and thus shown as a black diamond.

Figure 4

Thermal diffusivity values measured as sample FLN cooled from 1600 K (filled symbols) were higher than measurements made during heating (open symbols) until about 800 K, although those made upon cooling at lower temperatures, as well as room temperature *D* measured many days later (010=cross, 001=diamond), were lower than the original measurements due to cracks in the sample. Measurements made on (010), (001) and ⊥ are shown with squares, circles and triangles, respectively.

Figure 5

Inverse thermal diffusivities for samples (a) albite, (b) FSU, (c) FON, (d) FLN, (e) FBM and (f) FLL. Inflections in 1/*D* plots (short double lines) correspond to approximate positions of phase transitions marked, and long double lines show the expected position of the solidus (see Figure 1). Measurements made on (010), (001) and ⊥ are shown with squares, circles and triangles, respectively. Fits from Table 2 are shown as lines in figure 5e. Arrows in figures 5c and 5f show the decrease in *D* due to melting or premelting. Larger error bars for albite (001) reflect uncertainty due to extreme sample thickness.

Figure 6

Correlation of room temperature values of 1/*D* (averaged for the three orientations) with α_v. Because only two orientations were measured, sample FLC is not shown in the diagram. α_v was

calculated using data from two different sources, squares= Tribaudino et. al (2010) and circles = Hovis et al. (2010). Linear fits to samples with An<40 and An>40 are shown (grey=Tribaudino; black= Hovis).

Figure 7

$D^{-1}(T)$ using fits from Hofmeister et. al (2009) and $\alpha_L T$ calculated from unit cell parameters (Tribaudino et al. 2010) for albite to high temperature.

Figure 8

Heat capacities (dashed lines) are compared with thermal conductivities (various solid and dotted lines) for plagioclase samples. Albite heat capacity is show in black, and thermal conductivity is shown with heavy black line. Also shown are thermal conductivities of FON (heavy dark gray), FLN (long dash-dot), FBM (thin black), and FLL (heavy light gray), all calculated using data from Holland and Powell (1998). Most thermal conductivities calculated with volumes from Tribaudino et. al (2010) are similar, as shown for albite (dotted black). FON (gray dotted) shows more dissimilarity. Because *D* was only measured in two of the three orientations, *k* of FSU was not calculated.

Figure 9

Comparison of our data (shaded and outlined box) with data for labradorite (squares) and oligoclase (circles) samples from Magnitskiy (1971), and for labradorite samples (Linvill 1987) from Nain (squares with crosses), Lake St. John (squares with diagonals) and Lake County (open squares).

Figure 10

Summary of thermal diffusivity of important mineral families; plagioclase *D* values (triangles) are among the lowest of all rock forming minerals, both at room temperature (D_{298}) and at high temperature (D_{highT}). Plagioclase D_{highT} was measured at ~1350 K for all samples in this study (does not include albite). Data for all orientations of other minerals are plotted along with lines of best fit; data were taken from the following references and used the following values for D_{highT}: quartz (open squares), with highT value from β-quartz at ~1100 K (Branlund and Hofmeister 2007); olivine (gray diamonds), used "high temperature" *D* (Table 2 in Pertermann and Hofmeister 2006); clinopyroxene (black squares), used D_{sat} (Pertermann and Hofmeister 2008); orthopyroxene (square with X), used *D* at ~1200 K (Hofmeister, 2011); garnet (gray dots), used D_{sat} (Hofmeister 2006); spinel (black dots), used *D* at ~1000 K (Hofmeister 2007). Sanidine (D_{highT} at ~1200 K) and albite (D_{highT} at ~1075 K) mark the alkali feldspar (open circles) trend (from Pertermann et al. 2008 and Hofmeister et al. 2009, respectively). Only single crystals with high temperature measurements of multiple orientations were plotted. The lines of best fit for clinopyroxene and orthopyroxene overlap, and are labeled "pyroxene." Trends correlate with number of infrared (IR) modes as labeled.

Table 1. Plagioclase sample characteristics

Sample	Locality and source	Composition	Notes
albite*	Amelia Courthouse, VA	$Ab_{98.2}An_{0.2}Or_{1.6}$	$Q_{od}(C\bar{1})$ = .92[a] or 1[b] (pegmatitic)
FSU	unknown purchased from Gems 'N Rough	$Ab_{94}An_{5}Or_{1}$	Transparent green, gemmy. Few very small inclusions visible on 010.
FON	Hawk Mine, NC Smithsonian NMNH #R2898	$Ab_{78}An_{19}Or_{3}$	Colorless crystal with schiller with albite twins and unidentified 0.3-0.5 mm inclusions. $Q_{od}(C\bar{1})$ = .55 [b] (pegmatitic)
FLN	Tabor Island, Nain, Labrador, Canada purchased from Excalibur Mineral Co.	$Ab_{51}An_{47}Or_{2}$	Grey color with distinct albite twinning visible on (001). Ilmenite inclusions. Irridescence on (010) suggests Bøggild intergowth.
FLT	Tuléar Province, Madagascar	$Ab_{45}An_{52}Or_{2}$	"Peacock blue" color with ilmenite inclusions. Irridescence on (010) suggests Bøggild intergrowth.
FBM	Mexico purchased from Gems 'N Rough	$Ab_{39}An_{59}Or_{2}$	Large transparent yellowish crystal
FLC	Clear Lake, Utah Smithsonian NMNH #C5869	$Ab_{36}An_{63}Or_{1}$	Transparent yellow, gemmy.
FLL	Lakeview, Lake Co., Oregon purchased from Minerals Unlimited	$Ab_{33}An_{65}Or_{1}$	Labradorite phenocrysts in basalt. Sharp *a* and *b* reflections and diffuse *e* and *c* reflections[c]. $Q_{od}(I\bar{1})$ [a] = .56 or .67
anorthite	synthetic	An_{100}	Anorthite mat, polycrystalline and probably containing some glass.

*analyzed in a previous study (Hofmeister et al, 2009). Order parameters taken from [a] Angel et al (1990) and [b] Tribaudino et al (2010): $Q_{od}(C\bar{1})$ = 1 is completely ordered, 0 is completely disordered; $Q_{od}(I\bar{1})$ = 0 is $C\bar{1}$, 1 is $I\bar{1}$. [c]From single crystal x-ray analysis (Wenk, 1980).

Table 2. Fits for plagioclase: $1/D = A + B \times 10^{-3}T + C \times 10^{-6}T^2 + E \times 10^{-10}T^3$

Sample	D_{298}	A	B	C	E	fit to max temp (K)
FSU 010	1.270	0.12764	2.8317	-2.2983	7.089	1355
FSU 001	1.102	0.32587	2.4352	-1.867	5.5956	1355
FSU ⊥‡	0.933					
FON 010	0.919	0.37311	3.3609	-3.2593	11.28	1165
FON 001	0.979	0.1606	4.1008	-4.2673	16.196	1160
FON ⊥	0.868	-0.12683	5.9887	-6.1487	21.71	1165
FLN 010	0.892	0.87027	0.8544	0.56329	-5.3968	1315
FLN 001	0.956	0.8487	0.55316	1.031	-6.5271	1327
FLN ⊥	0.797	0.58276	2.8072	-1.7825	3.6512	1315
FLT010	0.780					
FLT001	0.882					
FLT⊥	0.758					
FBM 010	0.794	0.78365	2.1618	-1.8828	5.6729	1553
FBM 001	0.776	0.765	2.3826	-2.2863	8.1682	1553
FBM ⊥	0.632	0.97549	2.7887	-2.5002	7.9683	1357
FLC010	0.884					
FLC001	0.836					
FLL 010*	0.767	0.62803	3.1953	-3.1519	10.438	1350
FLL 001	0.751	0.94814	1.767	-1.6872	5.9099	1350
FLL ⊥**	0.811	0.63794	3.0079	-2.9822	9.7881	1350

In samples FON and FLL, measurements affected by melting onset were not included in fits. ‡Due to smalll sample size, FSU⊥ was measured at room temperature only. FLT, FLC and FAL were measured at room temperature, only. *R=0.988 and **R=0.97; for all other samples, fits are better than R=0.988.

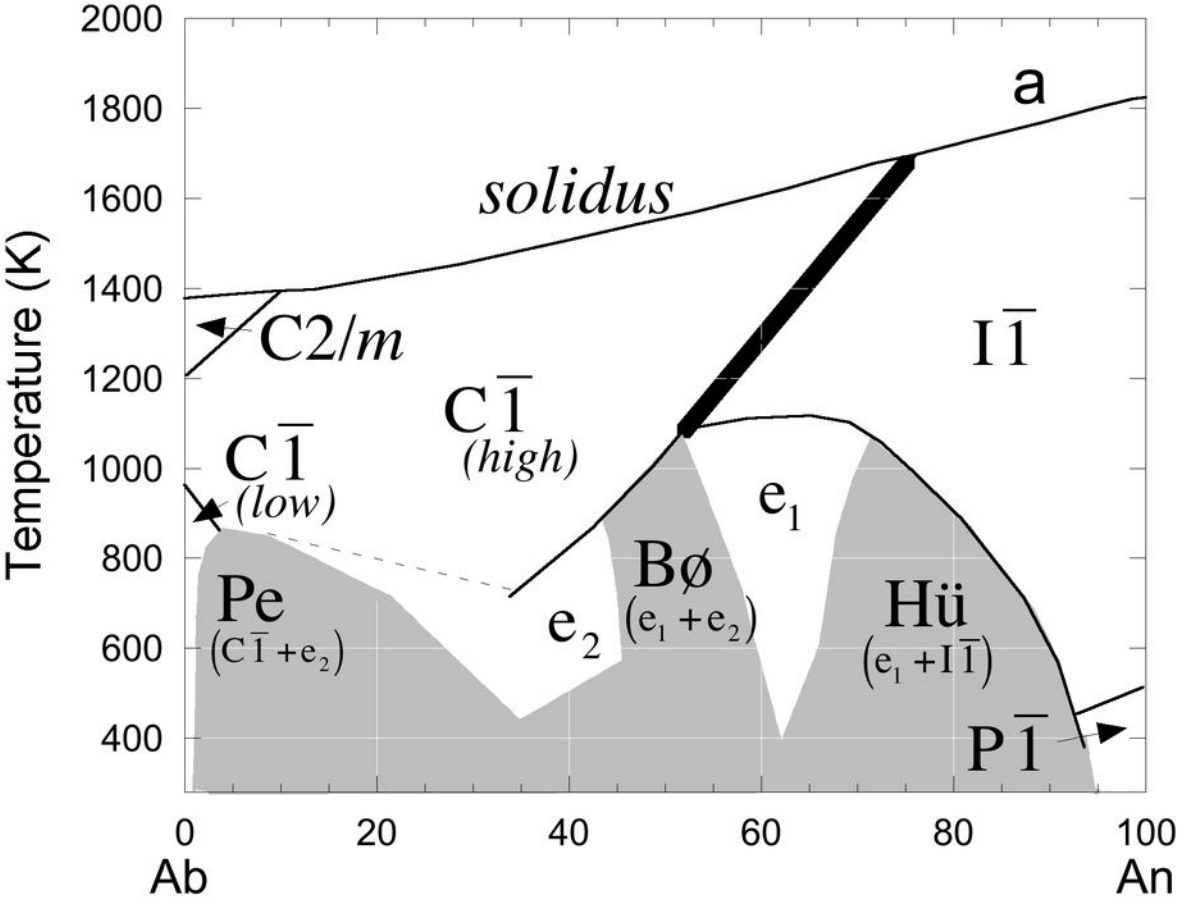
2000
1800
1600
1400
1200
1000
800
600
400
Temperature (K)
0
20
40
60
80
100
Ab
An
a
solidus
C2/m
I$\bar{1}$
C$\bar{1}$
(high)
C$\bar{1}$
(low)
e$_1$
Pe
(C$\bar{1}$ + e$_2$)
e$_2$
Bø
(e$_1$ + e$_2$)
Hü
(e$_1$ + I$\bar{1}$)
P$\bar{1}$

Figure 1

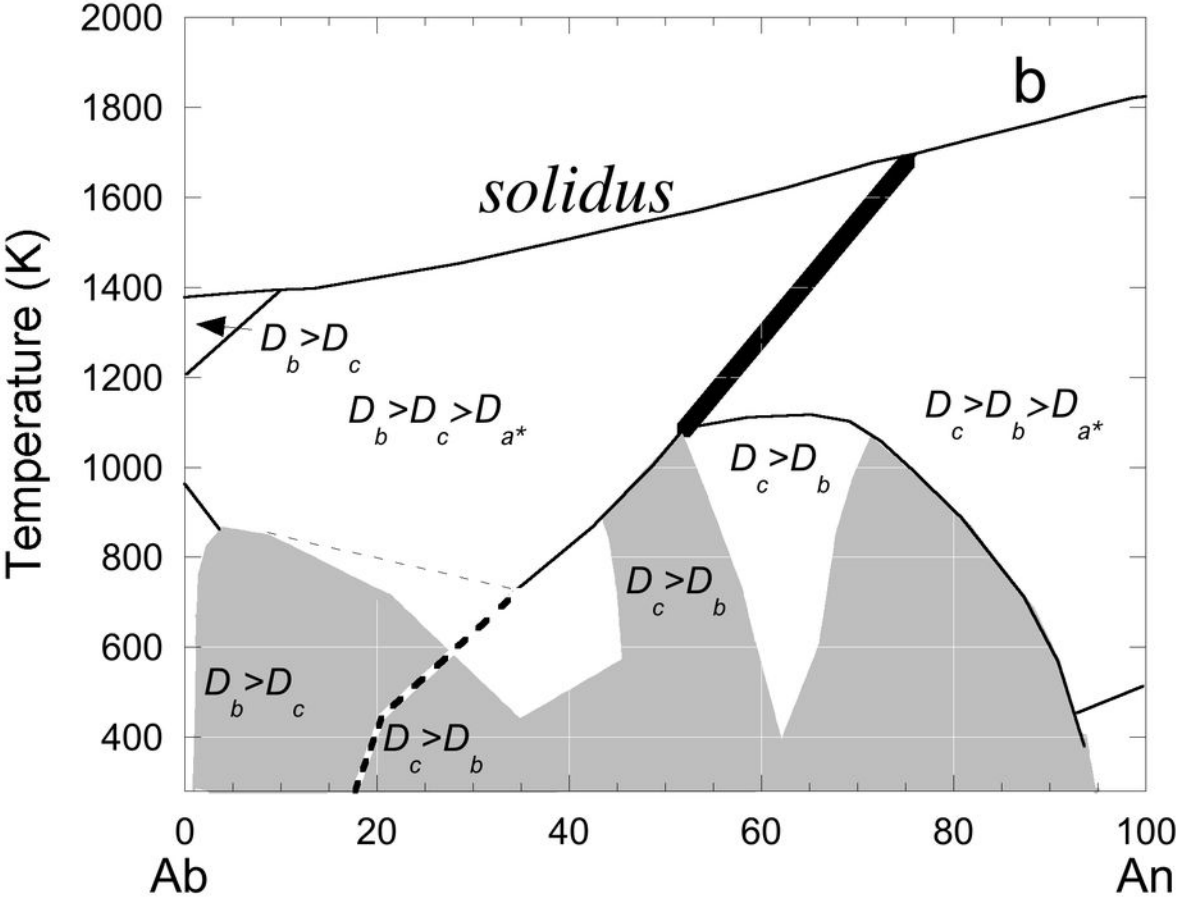
b
solidus
Temperature (K)
2000
1800
1600
1400
1200
1000
800
600
400
0
20
40
60
80
100
Ab
An
D b >D c
D b >D c >D a*
D c >D b >D a*
D c >D b
D c >D b
D b >D c
D c >D b

Figure 1

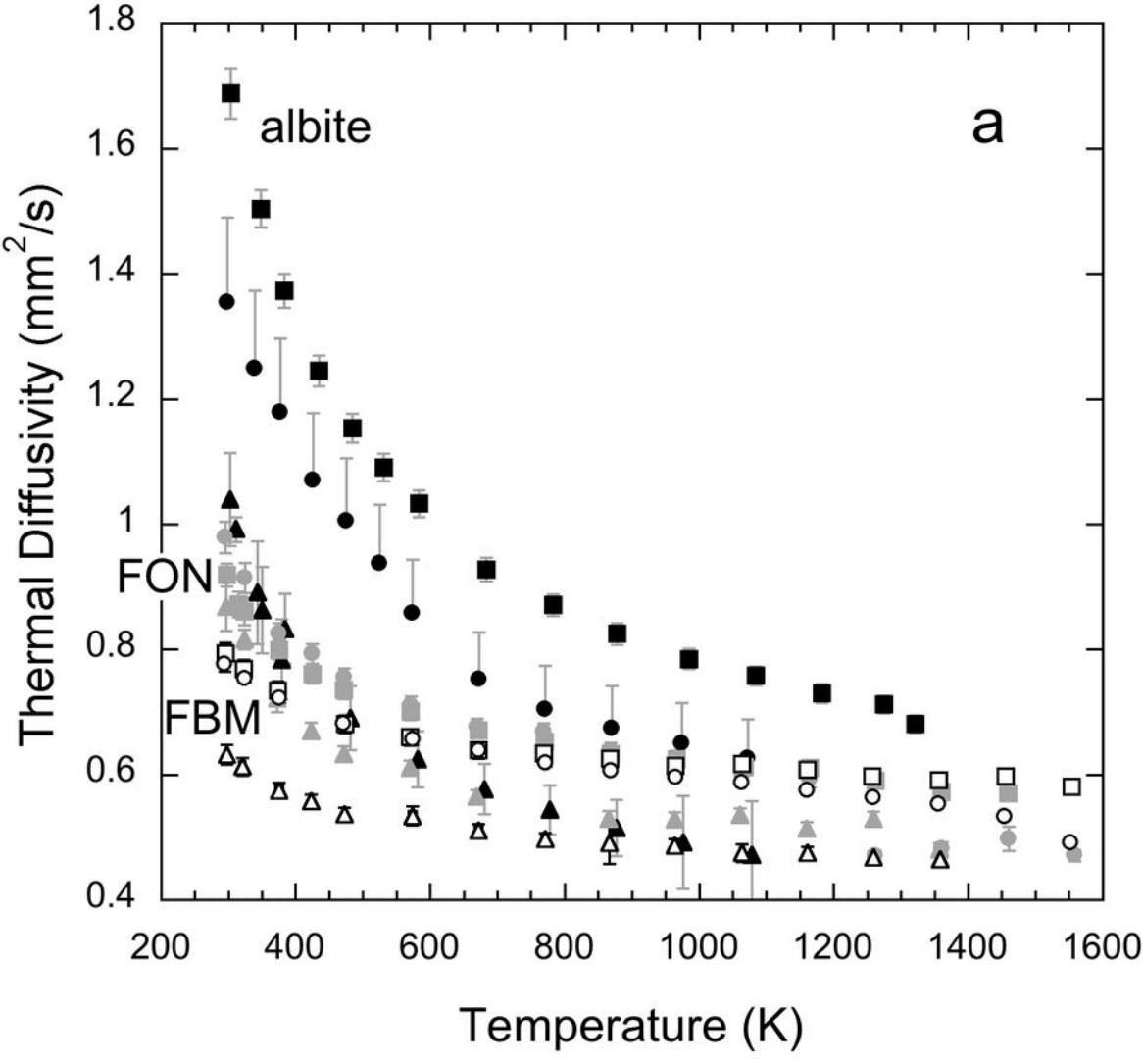
albite
a
FON
FBM
Thermal Diffusivity (mm^2/s)
Temperature (K)
1.8
1.6
1.4
1.2
1
0.8
0.6
0.4
200
400
600
800
1000
1200
1400
1600

Figure 2

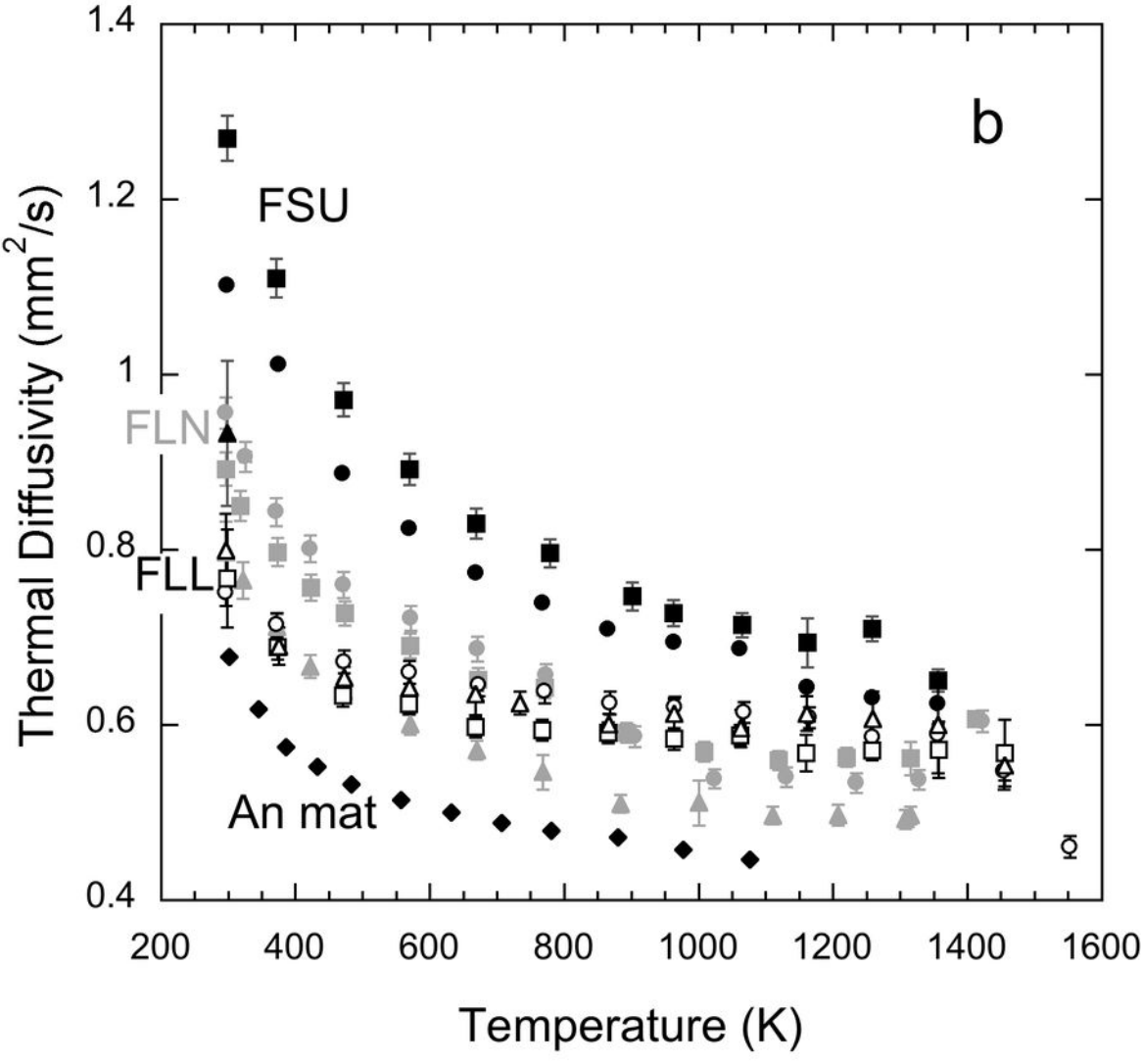
b
FSU
FLN
FLL
An mat
Thermal Diffusivity (mm^2/s)
Temperature (K)
1.4
1.2
1
0.8
0.6
0.4
200
400
600
800
1000
1200
1400
1600

Figure 2

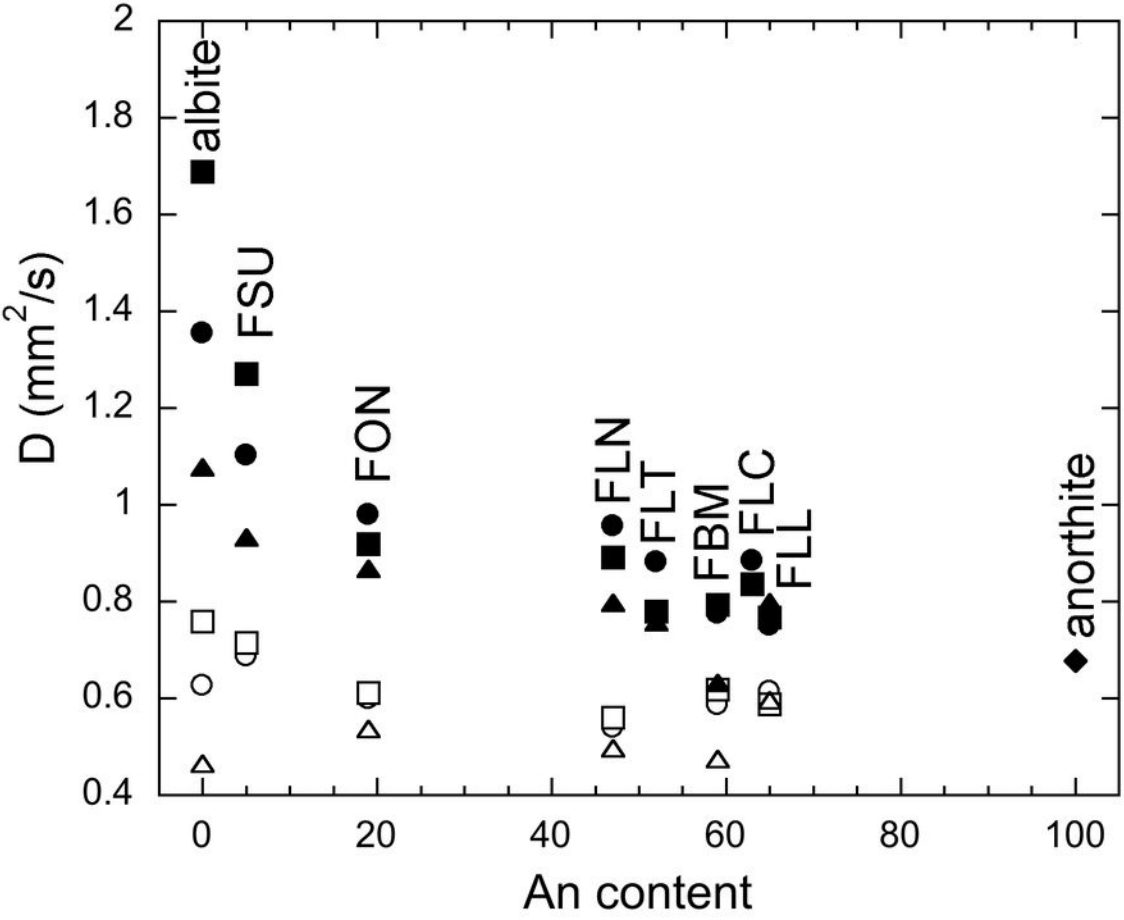
albite
FSU
FON
FLN
FLT
FBM
FLC
FLL
anorthite
D (mm²/s)
An content
2
1.8
1.6
1.4
1.2
1
0.8
0.6
0.4
0
20
40
60
80
100

Figure 3

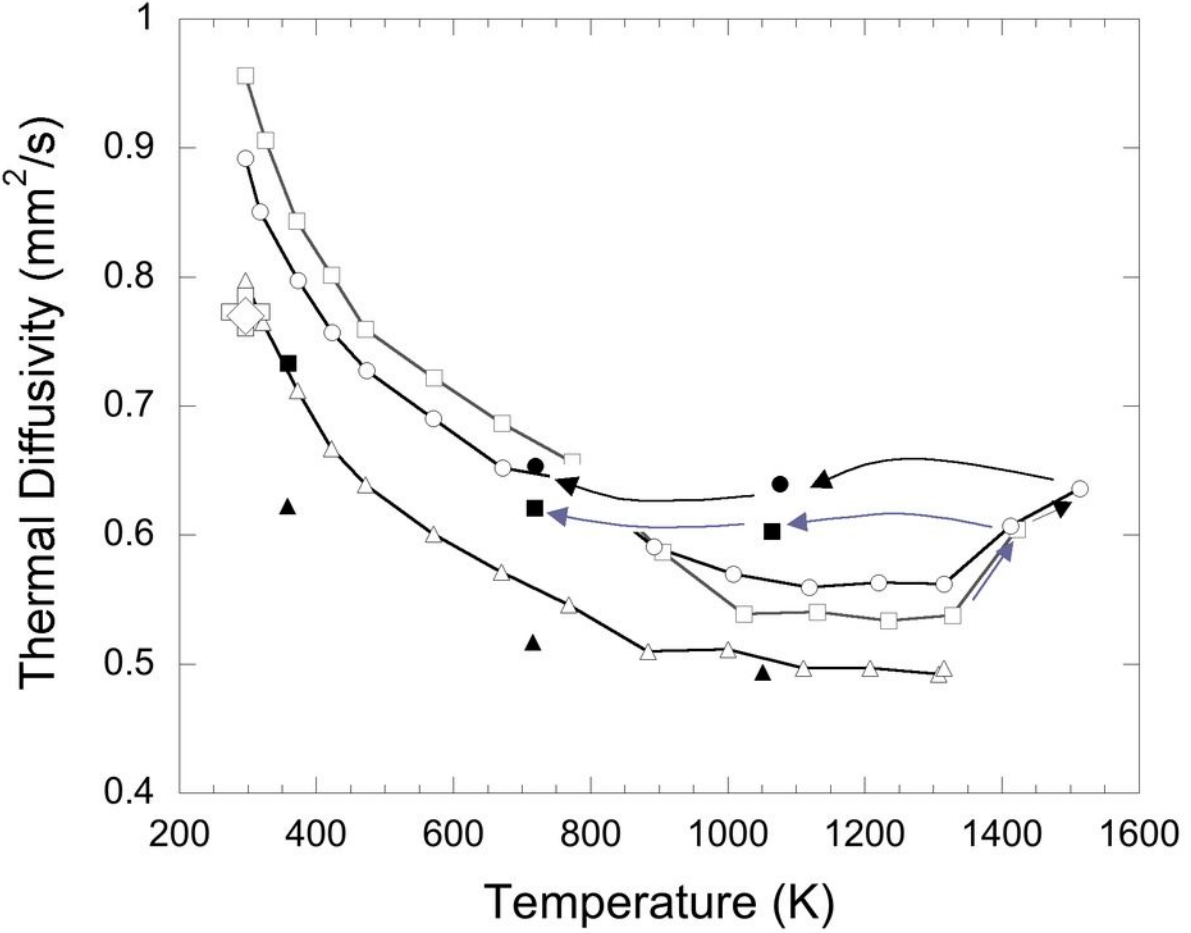
Thermal Diffusivity (mm^2/s)
1
0.9
0.8
0.7
0.6
0.5
0.4
200
400
600
800
1000
1200
1400
1600
Temperature (K)

Figure 4

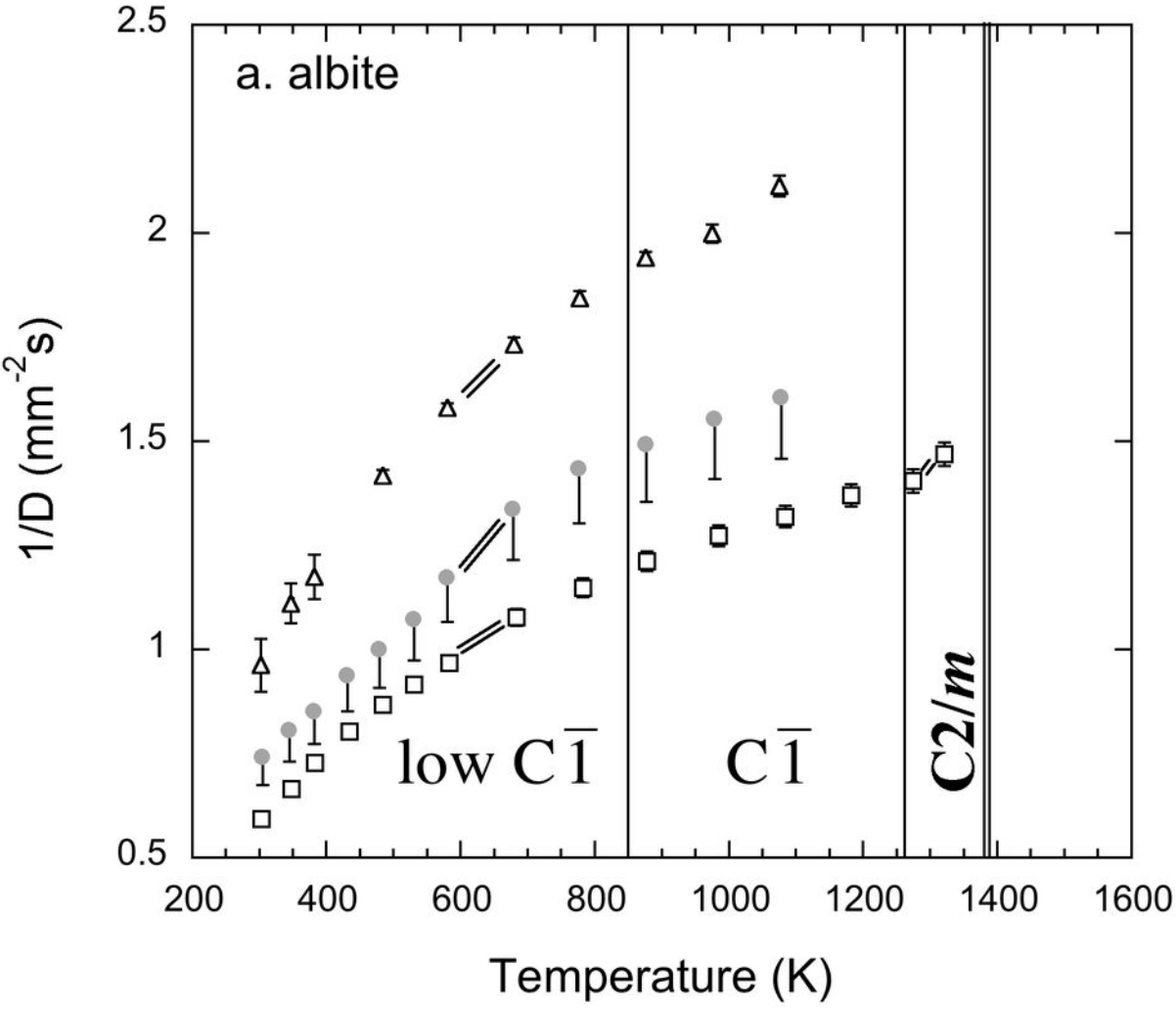
a. albite
low C$\bar{1}$
C$\bar{1}$
C2/m
1/D (mm^{-2}s)
Temperature (K)
2.5
2
1.5
1
0.5
200
400
600
800
1000
1200
1400
1600

Figure 5

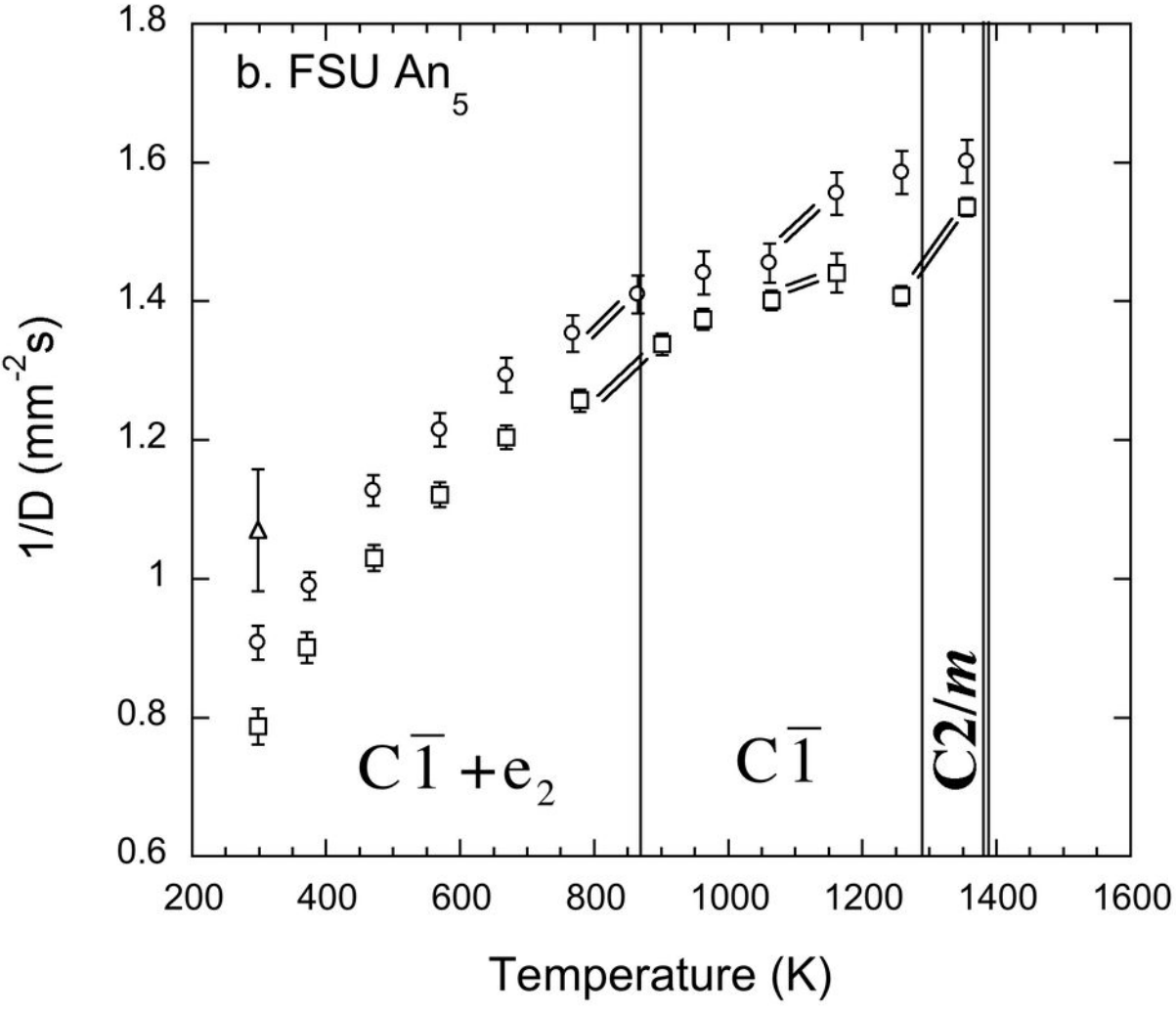
b. FSU An5
1/D (mm-2s)
Temperature (K)
C1̄ + e2
C1̄
C2/m
1.8
1.6
1.4
1.2
1
0.8
0.6
200
400
600
800
1000
1200
1400
1600

Figure 5

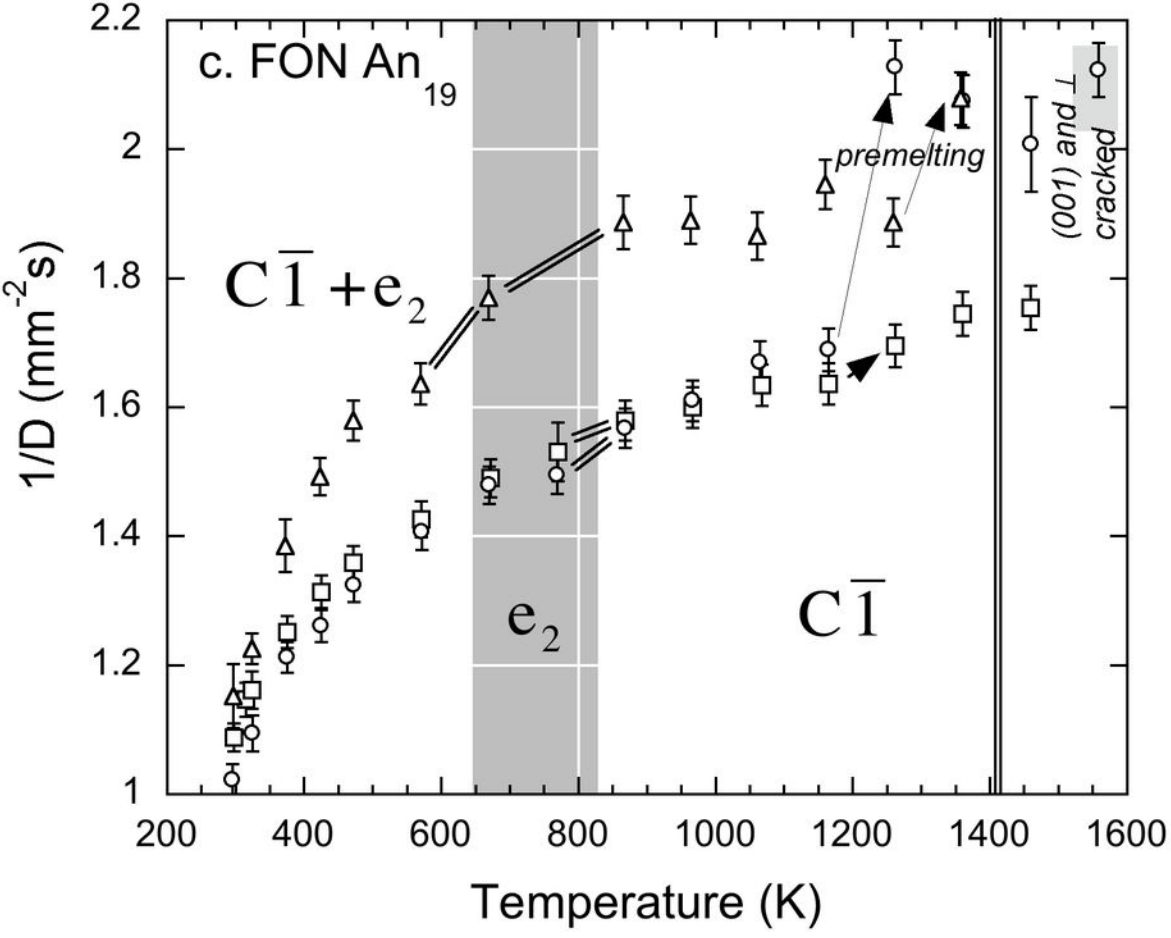
c. FON An19
premelting
(001) and ⊥ cracked
C1̄ + e2
e2
C1̄
1/D (mm-2s)
Temperature (K)
2.2
2
1.8
1.6
1.4
1.2
1
200
400
600
800
1000
1200
1400
1600

Figure 5

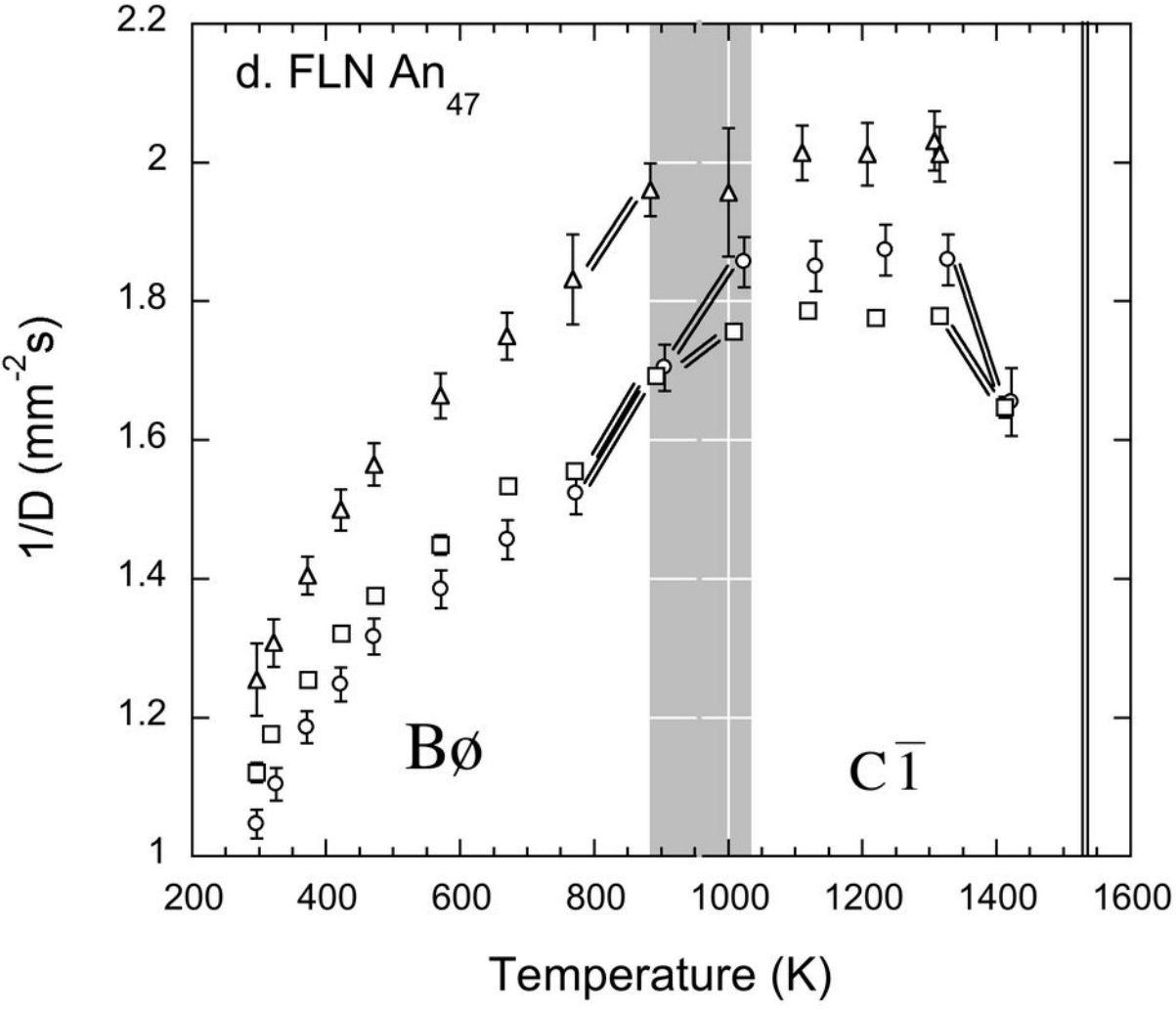
d. FLN An47
2.2
2
1.8
1.6
1.4
1.2
1
1/D (mm-2s)
200
400
600
800
1000
1200
1400
1600
Temperature (K)
Bø
C1̄

Figure 5

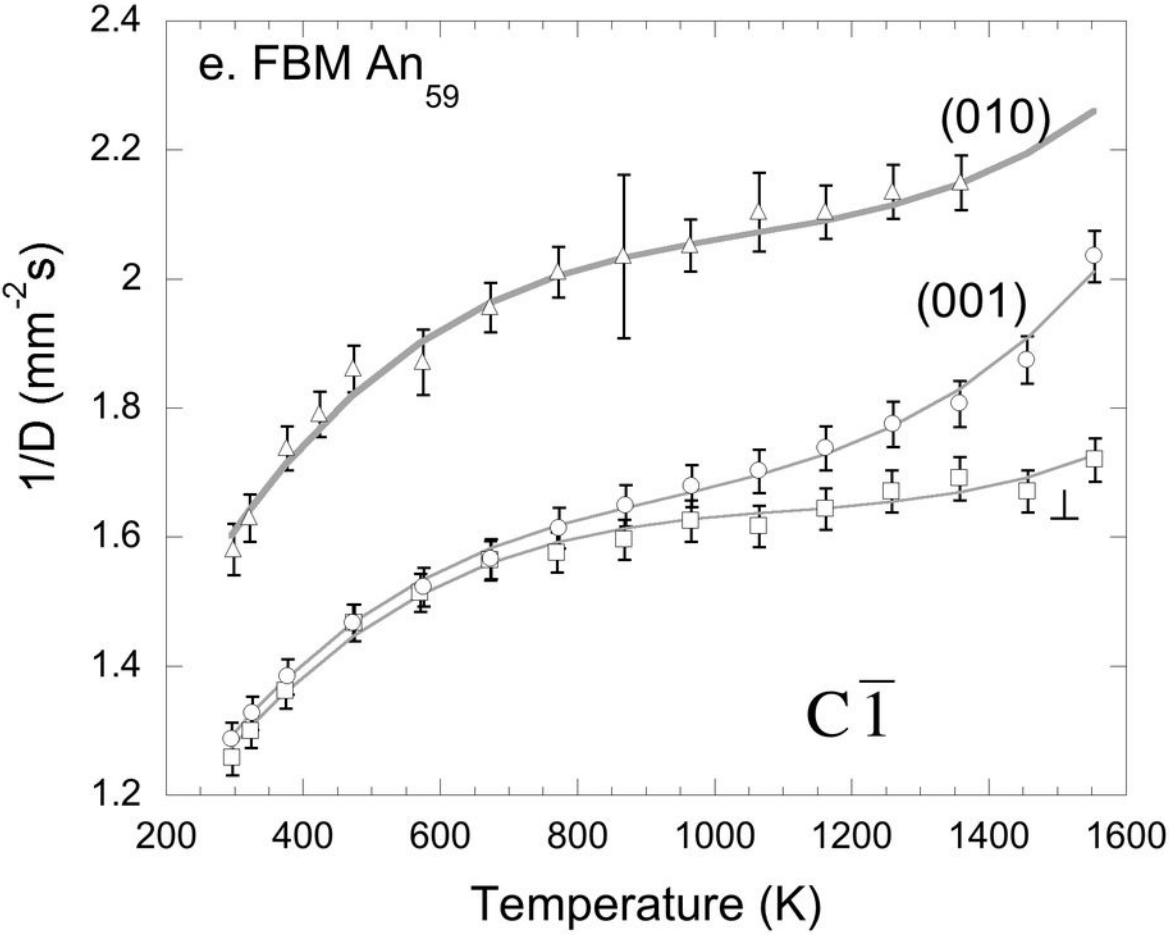
e. FBM An59
(010)
(001)
⊥
C1̄
1/D (mm-2s)
Temperature (K)
2.4
2.2
2
1.8
1.6
1.4
1.2
200
400
600
800
1000
1200
1400
1600

Figure 5

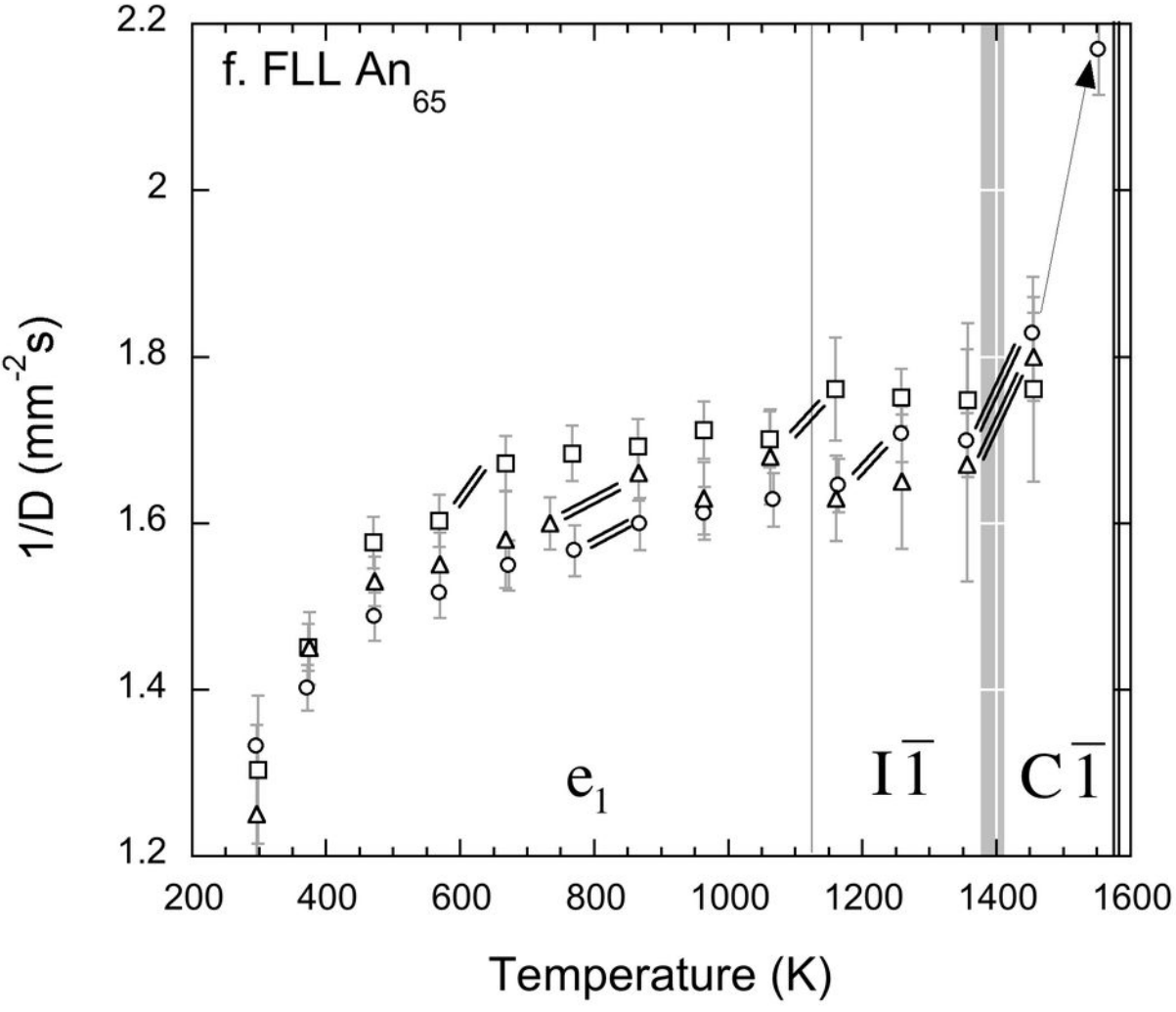
f. FLL An65
1/D (mm-2s)
Temperature (K)
e1
I1̄
C1̄
2.2
2
1.8
1.6
1.4
1.2
200
400
600
800
1000
1200
1400
1600

Figure 5

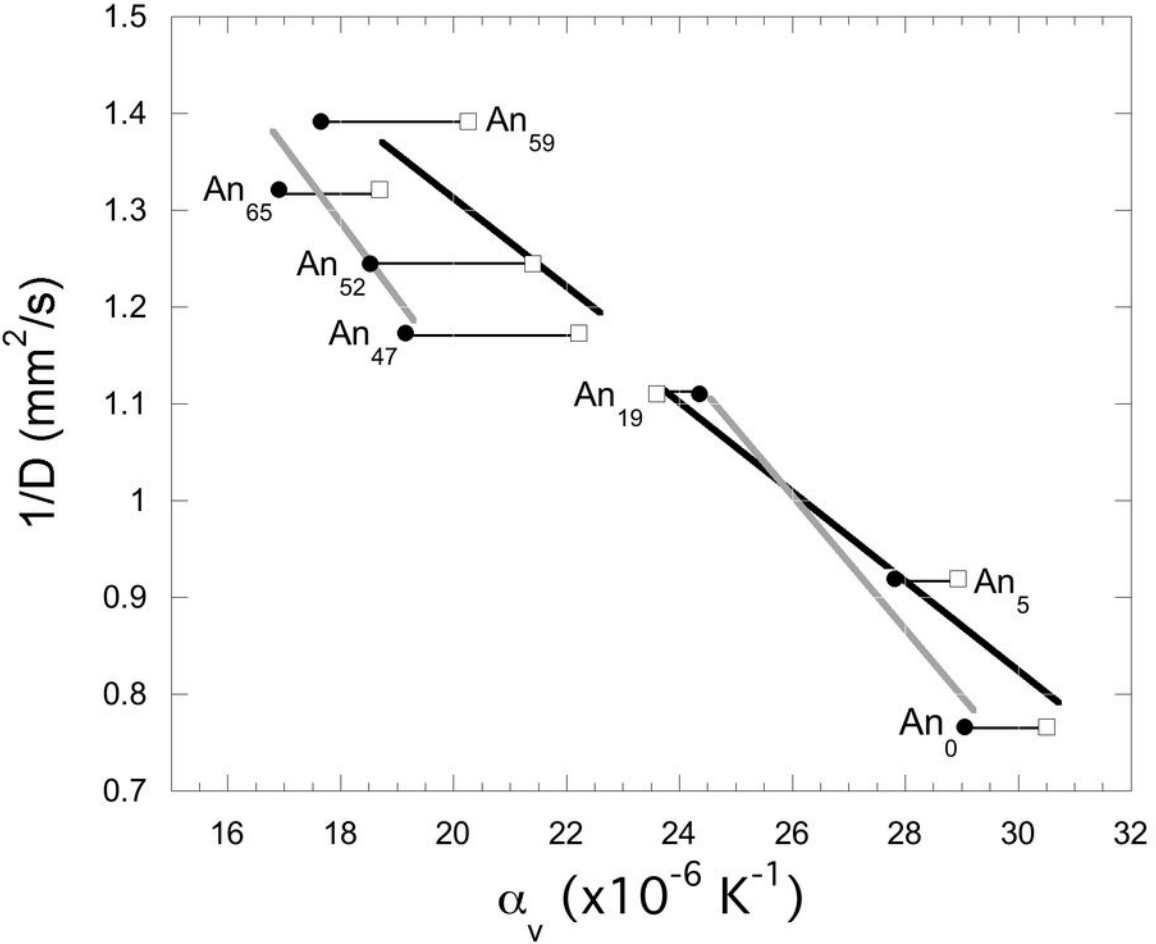
1.5
1.4
1.3
1.2
1.1
1
0.9
0.8
0.7
1/D (mm²/s)
An59
An65
An52
An47
An19
An5
An0
16
18
20
22
24
26
28
30
32
αv (x10⁻⁶ K⁻¹)

Figure 6

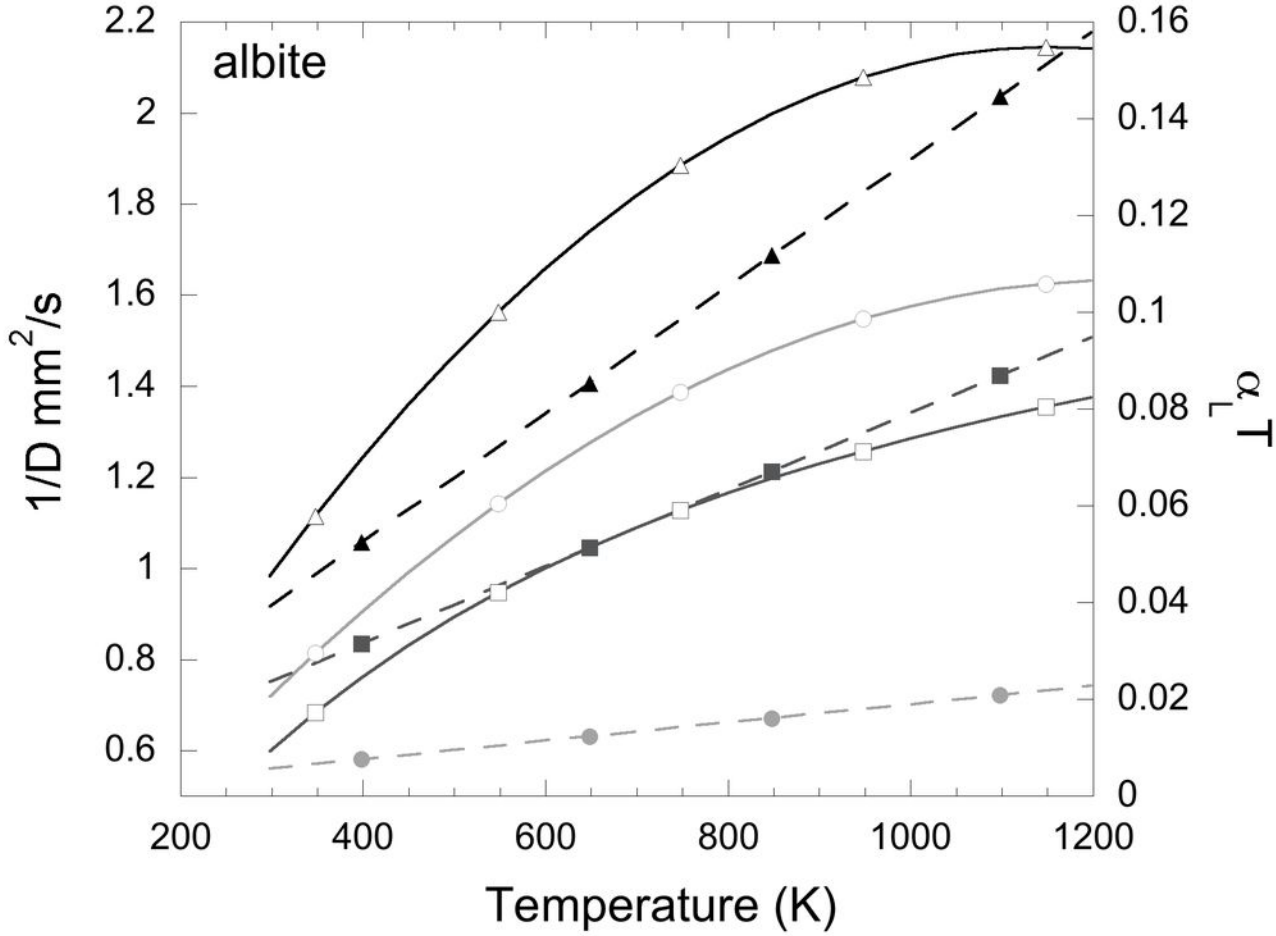
albite
1/D mm^2/s
$\alpha_L T$
Temperature (K)
2.2
2
1.8
1.6
1.4
1.2
1
0.8
0.6
0.16
0.14
0.12
0.1
0.08
0.06
0.04
0.02
0
200
400
600
800
1000
1200

Figure 7

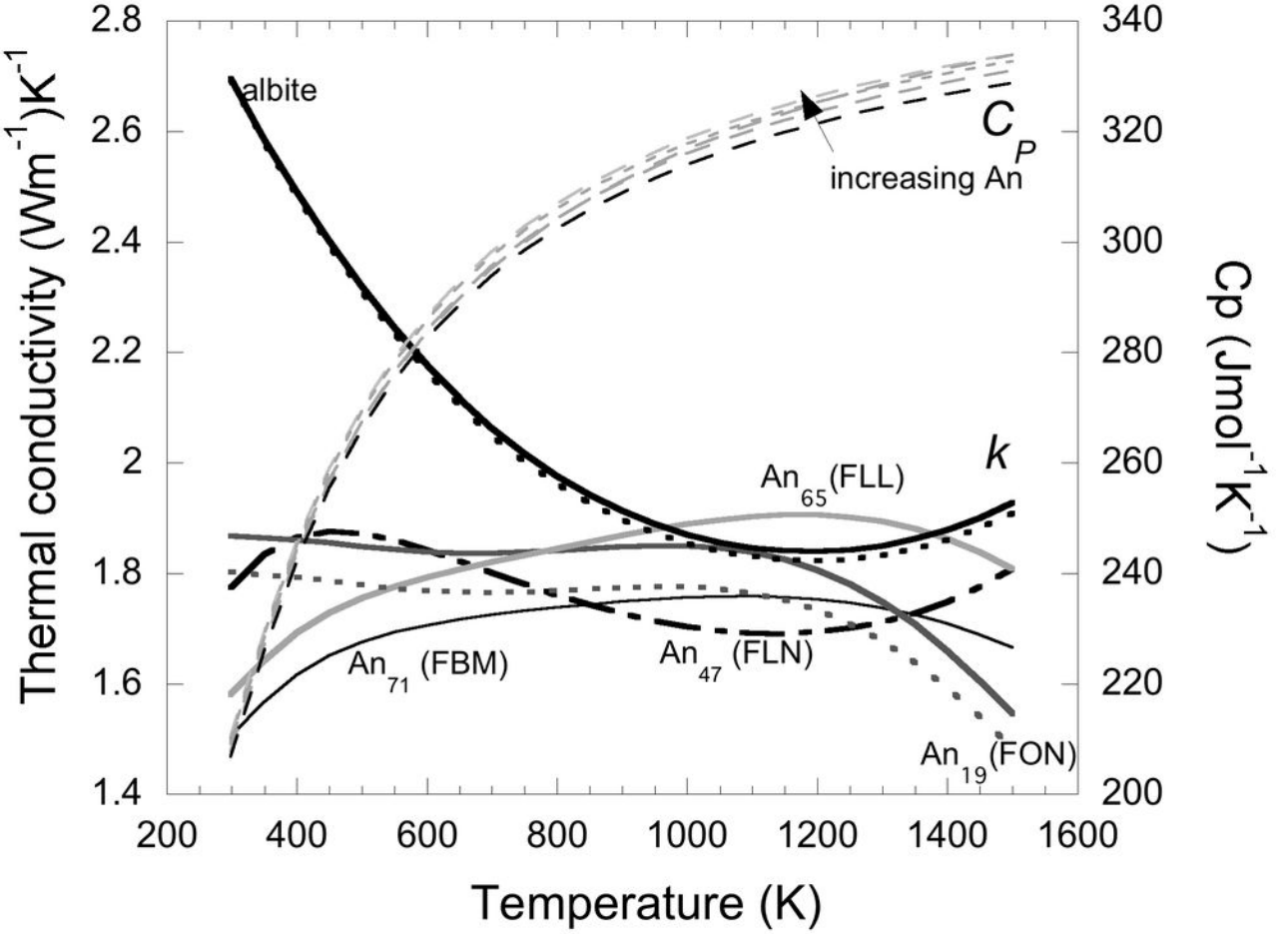
albite
C_P
increasing An
k
An_{65}(FLL)
An_{71} (FBM)
An_{47} (FLN)
An_{19}(FON)
Thermal conductivity (Wm^{-1})K^{-1}
Cp ($Jmol^{-1}K^{-1}$)
Temperature (K)
2.8
2.6
2.4
2.2
2
1.8
1.6
1.4
340
320
300
280
260
240
220
200
200
400
600
800
1000
1200
1400
1600

Figure 8

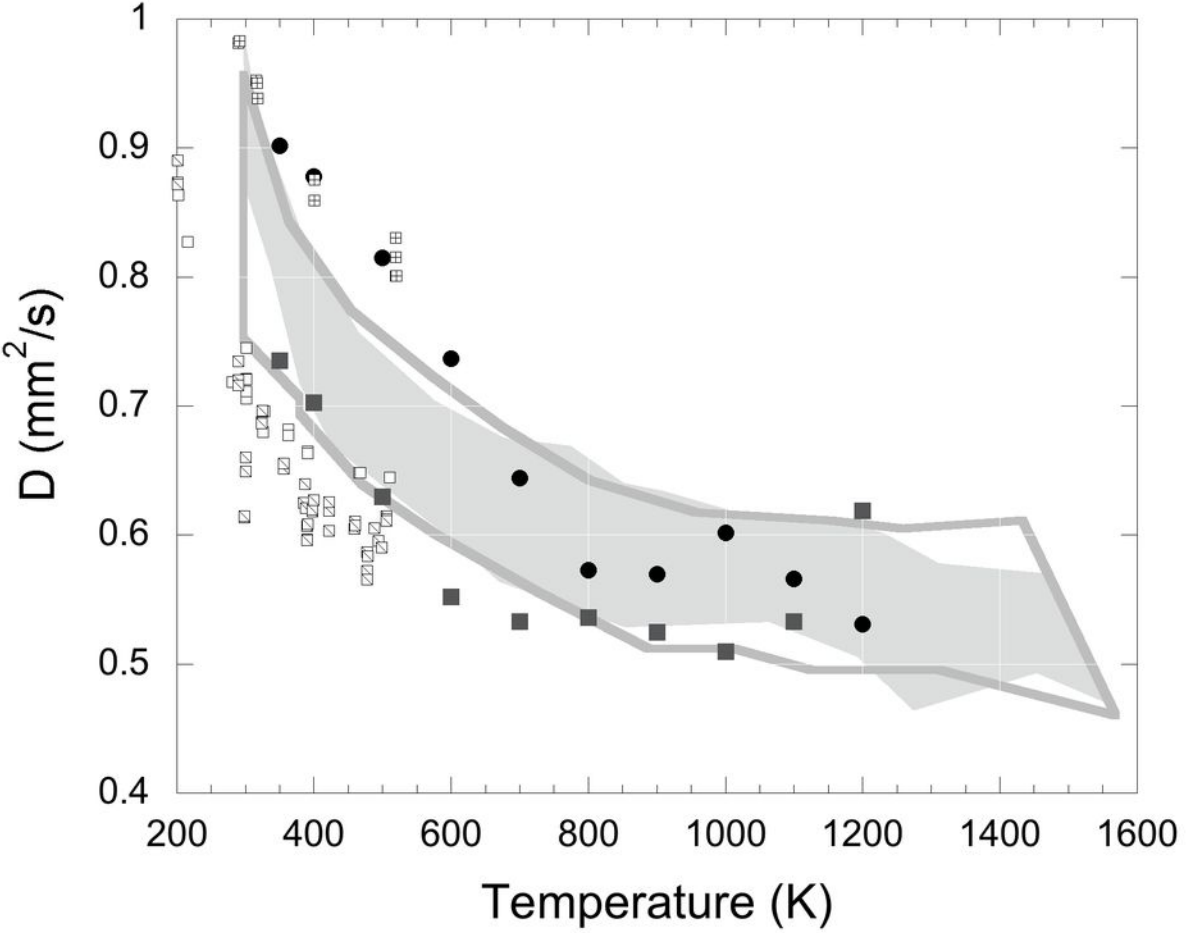
1
0.9
0.8
0.7
0.6
0.5
0.4
D (mm^2/s)
200
400
600
800
1000
1200
1400
1600
Temperature (K)

Figure 9

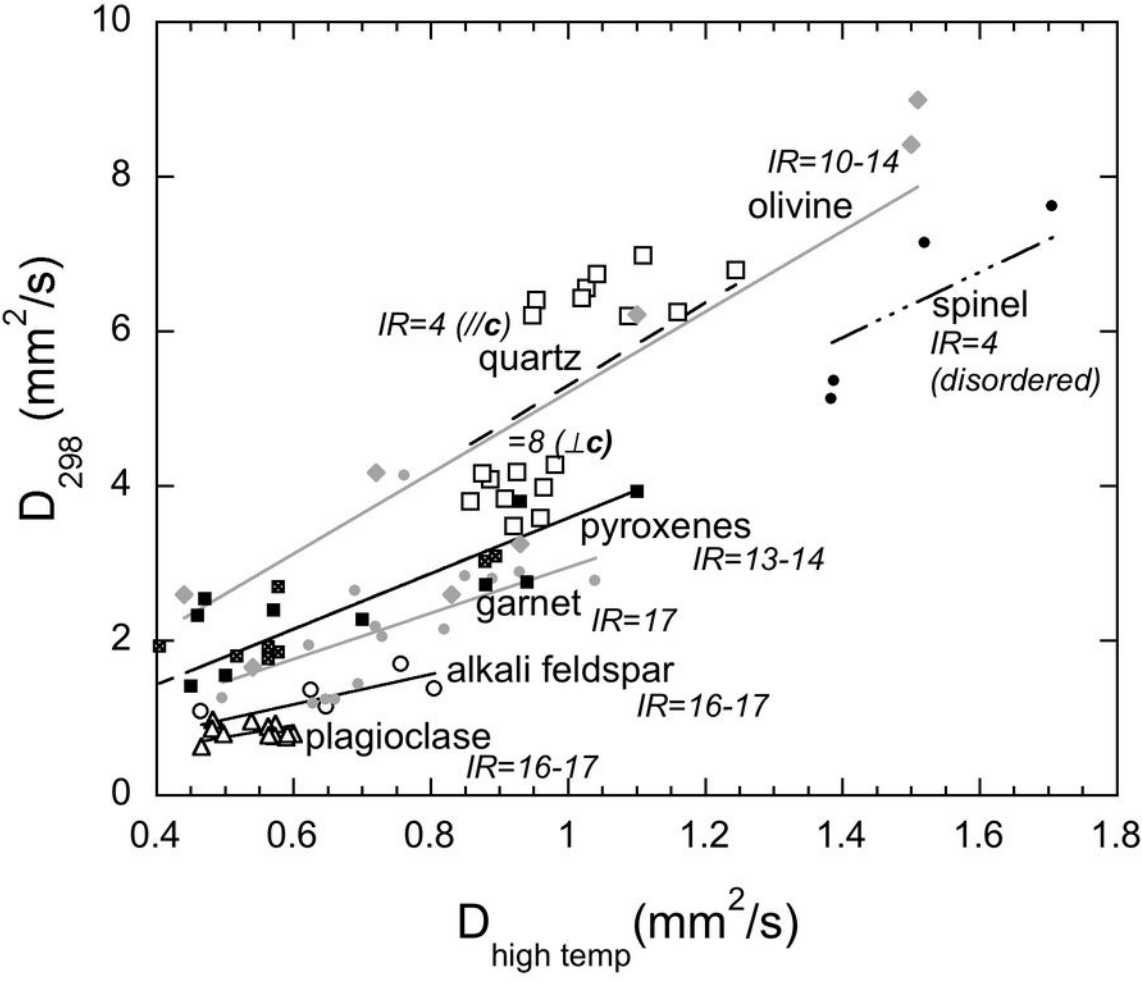
10
8
6
4
2
0
0.4
0.6
0.8
1
1.2
1.4
1.6
1.8
D298 (mm2/s)
Dhigh temp (mm2/s)
IR=10-14
olivine
IR=4 (//c)
quartz
=8 (⊥c)
spinel
IR=4
(disordered)
pyroxenes
IR=13-14
garnet
IR=17
alkali feldspar
IR=16-17
plagioclase
IR=16-17

Figure 10